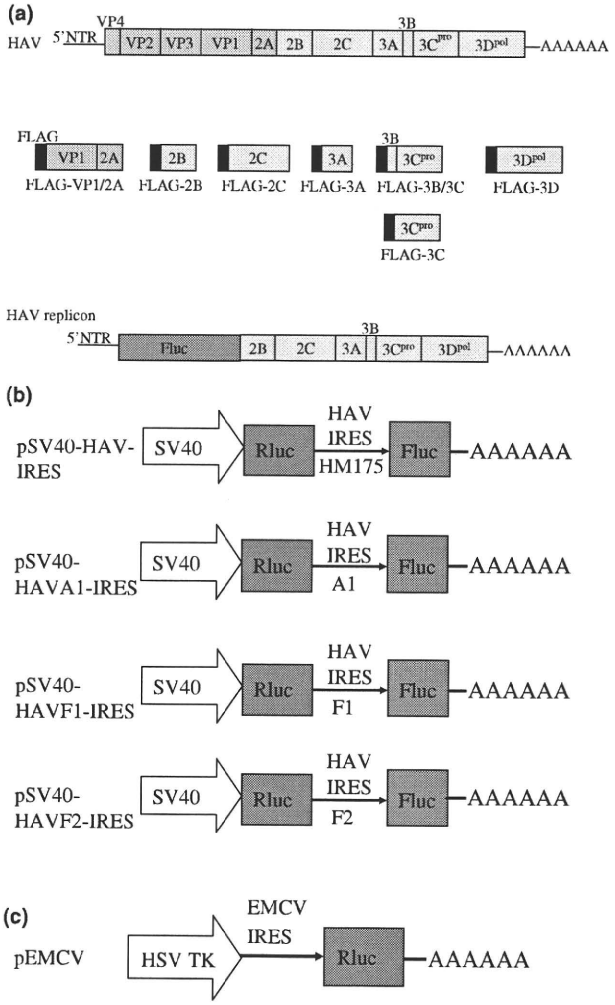


**Fig. 1** Schematic representation of the hepatitis A virus (HAV) constructs used in this study. (a) Structures of the HAV genome (upper panel), FLAG-tagged HAV proteins (middle panel; ref. 17) and HAV replicon pT7-18f-luciferase (lower panel; ref. 13). AAAAAA, poly A tail. (b) Structure of the bicistronic plasmids used. pSV40-HAV-internal ribosome entry site (IRES) encodes the Renilla luciferase, the IRES of HAV strain HM175 and the firefly luciferase (Fluc) under the control of the simian virus 40 promoter (SV40) (ref. 16). pSV40-HAVA1-IRES, pSV40-HAVF1-IRES and pSV40-HAVF2-IRES encode IRES elements derived from an acute hepatitis and two fulminant hepatitis cases, respectively. (c) Structure of plasmid pEMCV.

competes with cap-dependent translation of host proteins [1,12]. In this study, we show that HAV $3C^{pro}$ cleaved PTB and suppressed cap-independent translation initiation. The data indicate that the viral proteinase might play an important role in the regulation of HAV IRES-mediated cap-independent translation by targeting noncanonical translation factors.

## MATERIALS AND METHODS

### *Cell lines*

Huh-7, a human hepatoma cell line, and its stably transformed derivative Huh-T7 that expresses the T7 RNA polymerase [3] were grown in Dulbecco's modified Eagle medium (Gibco BRL, Gaithersburg, MD, USA) supplemented with 10% heat-inactivated foetal bovine serum with or without G418 sulfate (400 μg/mL; Promega, Madison, WI, USA), in addition to penicillin and streptomycin.

### *Plasmids*

pT7-18f-luciferase (LUC), a replication-competent HAV replicon, containing an open-reading frame with the firefly luciferase (Fluc) flanked by the first four amino acids of the HAV polyprotein and by 12 C-terminal amino acids of VP1, followed by the P2 and P3 domains of the HAV polyprotein (HAV strain HM175 18f, GenBank Accession No. M59808), and pT7-18f-LUCmut, a replication-deficient replicon, were described previously [13] (Fig. 1a).

The constructs encoding the simian virus 40 (SV40) promoter-driven *Renilla reniformis* luciferase (Rluc), the IRES derived from the cell culture adapted HAV strain HM175 [14], and Fluc, named pSV40-HAV-IRES, was prepared as described previously [2,15] (Fig. 1b). To investigate the specific effect exerted by the HAV IRES sequences, bicistronic reporter constructs (pSV40-HAVA1-IRES, pSV40-HAVF1-IRES and pSV40-HAVF2-IRES; Kanda *et al.*, manuscript in preparation) were prepared, which included the IRES of clinical specimens. Construction of HAV protein expression plasmids was described previously [16]. Briefly, seven regions of the HAV genome were amplified by reverse transcription-polymerase chain reaction (PCR) with HAV region-specific primers [16]. These regions were HAV VP1-2A, 2B, 2C, 3A, 3BC, 3C and 3D. The amplified products were cloned into pCXN2 (kindly provided by Prof. J. Miyazaki, Osaka University, Japan), a mammalian expression vector with a beta-actin-based CAG promoter and a SV40 origin [17], to generate pCXN2-FLAG-VP1-2A, 2B, 2C, 3A, 3BC, 3C, 3D expressing FLAG-tagged proteins [16] (Fig. 1a). To control for the target specificity, pEMCV, which contains the encephalomyocarditis virus (EMCV) IRES upstream of Rluc, was generated (Fig. 1c). Transient expression of $3C^{pro}$ using vaccinia virus, pGEM-3C, and pEXT7-HAV3C was described before [12].

### *Transfection and protein analyses*

Approximately 60% confluent Huh-7 cells, grown in 6-well culture plates, were transfected with 0.3 μg of the LUC reporter plasmid and 0.1 μg of each HAV protein-expressing plasmid using Effectene transfection reagent (Qiagen, Tokyo, Japan). Forty-eight hours after transfection, cell

extracts were prepared, and a LUC assay kit (Toyo Ink, Tokyo, Japan) was used according to the manufacturer's instructions. LUC activity was measured in relative light units with a luminometer (AB-2200-R; ATTO, Tokyo, Japan). The assays were adjusted to protein amount and were conducted, on average, in duplicate [18]. To determine cleavage of the host proteins PTB and poly(A)-binding protein (PABP), extracts of transfected cells were analysed for viral antigen and host proteins, as described previously [12]. Viral proteins were identified using anti-FLAG and anti-HAV 3C antibodies. PTB was recognized by the monoclonal antibody BB7 [19].

## RESULTS

### *HAV proteinases 3BC and 3C suppress IRES-dependent translation*

Translation of the HAV polyprotein is initiated cap-independently and is driven by an IRES. As a first approach to assess the role of HAV proteins, we examined cap-independent and cap-dependent translation using the bicistronic reporter constructs depicted in Fig. 1. pSV40-HAV-IRES, which contains the IRES of HAV strain HM175 (Fig. 1b), was transfected into Huh-7 together with various expression vectors encoding FLAG-tagged HAV protein (Fig. 1a). The expression of these proteins was confirmed by Western blotting with anti-FLAG antibodies (data not shown and ref. 16). Compared to the control (pCXN2) and to the other HAV proteins tested (VP1-2A, 2B, 2C, 3A and 3D), expression of HAV 3BC or 3C specifically inhibited cap-independent translation initiated by the HAV IRES as determined by the Fluc activity (Fig. 2).

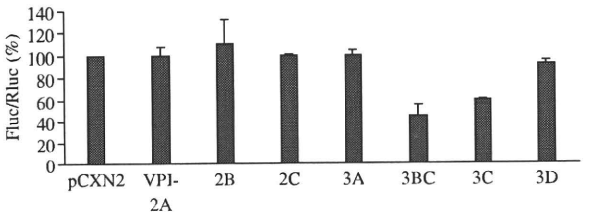


**Fig. 2** Effects of hepatitis A virus (HAV) proteins on HAV internal ribosome entry site (IRES)-dependent translation. Relative luciferase activities are indicated (IRES/Cap; firefly luciferase/*Renilla reniformis* luciferase, %). Luciferase activities were determined in three independent experiments. Error bars represent standard errors of the mean.

To corroborate the observed suppression of HAV IRES-independent translation, we next examined the effect of $3C^{pro}$ on translation, which was dependent on HAV IRES elements derived from clinical isolates; IRES A1 was taken from an acute self-limited hepatitis (pSV40-HAVA1-IRES), and F1 and F2 were derived from fulminant HAV infections (pSV40-HAVF1-IRES and pSV40-HAVF2-IRES) (Fig. 3a–c). After coexpression of pSV40-HAVA1-IRES, pSV40-HAVF1-IRES and pSV40-HAVF2-IRES with 3BC or $3C^{pro}$, the Fluc activity was specifically suppressed when compared to the control (pCXN2, Fig. 3a–c). The results confirm our findings shown in Fig. 2 and demonstrate that HAV proteinases 3BC and $3C^{pro}$ suppress HAV IRES-dependent translation. For yet unknown reasons, the negative effect of 3BC was generally more pronounced than that exerted by $3C^{pro}$. However, as $3C^{pro}$ is the prevailing and stable form of the viral proteinase, only this form was used in the subsequent studies.

Translation of the viral polyprotein is the first metabolic step in the viral life cycle and a prerequisite for viral RNA synthesis. It can be assumed that a negative effect on

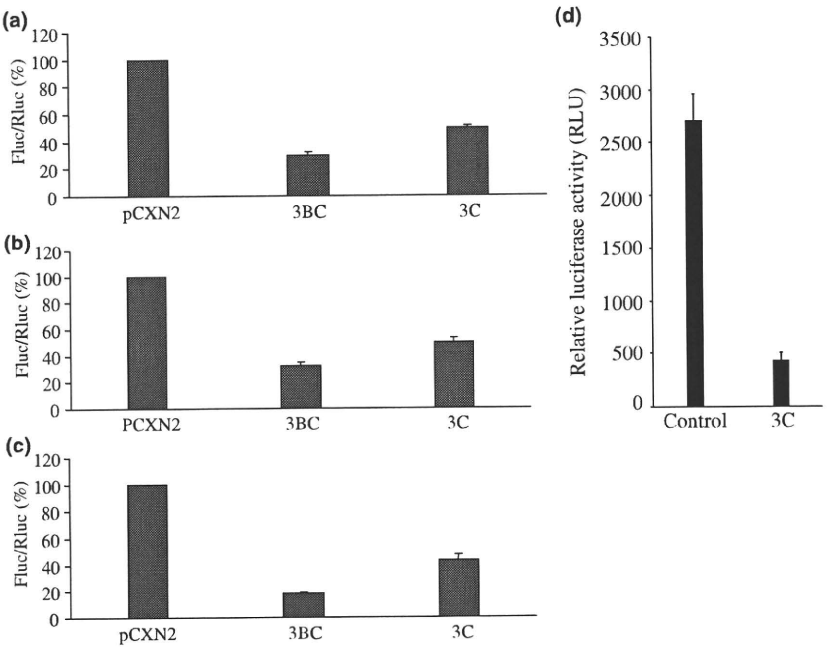


**Fig. 3** Effects of hepatitis A virus (HAV) 3BC or $3C^{pro}$ on HAV internal ribosome entry site (IRES)-dependent translation (a–c) and on expression of the HAV replicon [pT7-18f-luciferase (LUC)] (d). HAV was derived from clinical isolates: (a) acute hepatitis; (b) and (c) two forms of fulminant hepatitis. Relative luciferase activities are indicated (IRES/Cap; firefly luciferase/*Renilla reniformis* luciferase, %) (a–c). LUC activities are presented as an average of three independent experiments. Error bars represent standard errors of the mean. RLU, relative light units.

translation might indirectly cause a reduction in viral genome production. HAV replication was efficiently studied using the viral replicon (see Fig. 1a, lower panel) with Fluc as reporter gene in place of the viral structural proteins [13]. The reporter gene activity is directly proportional to viral RNA synthesis. To investigate whether 3C-mediated suppression of translation affects genome replication, we cotransfected HAV replicon RNA with the 3C-expression or control vector into Huh-T7 cells (Fig. 3d). HAV replicon replication was monitored by reporter assay 72 h post-transfection. Compared to the replication-deficient replicon (pT7-18f-LUCmut), the reporter activity at this point was derived from newly synthesized viral genomes and therefore represents viral genome synthesis [13]. Compared to the control, HAV replication was significantly suppressed in the presence of excess 3C, indicating that 3C-mediated inhibition of translation restrained HAV genome replication in human hepatoma cells.

To assess the specificity of the inhibitory effect exerted by HAV proteinase $3C^{pro}$, translation initiated at the EMCV IRES was compared with the HAV IRES. For this, HAV $3C^{pro}$ was coexpressed with pEMCV (Fig. 1c), and the Rluc activity of the cell extracts collected 48 h post-transfection was determined. Compared to the HAV IRES tested in parallel experiments, the EMCV IRES activity was similar in the presence and absence of coexpressed HAV $3C^{pro}$ [118 ± 29 (%)]. Combined and in light of the results described in the following, these findings suggest that an essential ITAF was cleaved by HAV $3C^{pro}$. As shown in the following, HAV $3C^{pro}$ partially cleaved PTB, whose active role in picornaviral IRES-dependent translation has been demonstrated previously [6,8]. As EMCV IRES translation was unaffected by HAV $3C^{pro}$, PTB is not an essential ITAF for this IRES, confirming an earlier report [20]. Intriguingly, an excess of PTB even suppressed EMCV IRES-driven translation [21]. The abundance and distribution of PTB varies significantly among cell types [6,8]. Large amounts of PTB were found in the cytoplasmic fraction of Huh-7 cells that were used in our studies. Based on these observations, the results reported here suggest that HAV $3C^{pro}$ reduced the cytoplasmic levels of intact PTB to such a degree that only the activity of the HAV IRES was affected, but not that of the EMCV IRES.

### *$3C^{pro}$ cleaves PTB*

It has been reported that the HAV IRES is associated with La autoantigen, GAPDH, PTB, PABP and PCBP [6,8,12–14]. The latter two proteins were cleaved by HAV $3C^{pro}$ [12,13]. Furthermore, it was shown that PTB is cleaved by polioviral $3C^{pro}$ and that PTB fragments inhibit polioviral IRES-dependent translation [22]. To assess whether the observed suppression of HAV IRES translation might be because of 3C-mediated cleavage of PTB, we tested the levels of endogenous PTB after transient expression of $3C^{pro}$ in Huh-7 cells. As GAPDH was found to suppress HAV IRES translation and to antagonize the enhancing effect of PTB [8], GAPDH levels were tested in parallel. As control for the proteolytic activity of $3C^{pro}$ *in vivo*, cleavage of the poly(A)-binding protein was also analysed. Recombinant $3C^{pro}$ was identified by immunoblot with anti-3C (Fig. 4, left panel) [12,13], and PABP was partially cleaved as demonstrated earlier (Fig. 4, middle panel). Whereas the levels of GAPDH were unchanged (data not shown), a PTB cleavage product of approximately 45 kDa and a slightly faster migrating polypeptide were clearly detectable when HAV $3C^{pro}$ was expressed (Fig. 4, right panel). The extent of host protein cleavage significantly depended on the amount of 3C expressed (compare lanes 1 and 3). Specific PTB cleavage was also observed when the extracts used in Fig. 2 were tested (not shown). Moreover, PTB of Huh-7 cells, the rabbit

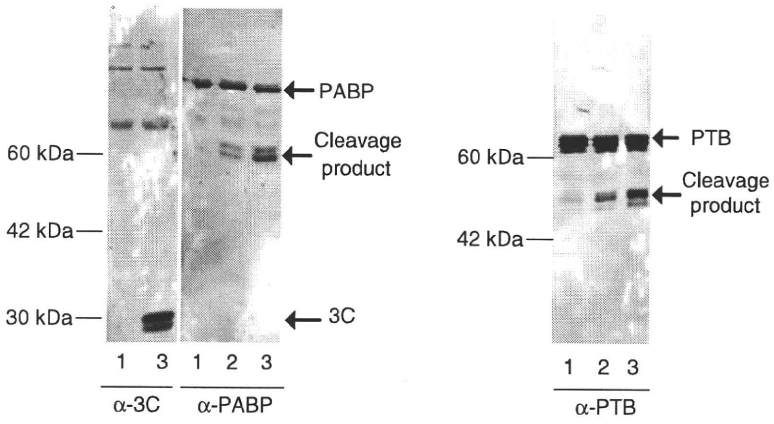


**Fig. 4** Hepatitis A virus (HAV) $3C^{pro}$ cleaves the polypyrimidine tract-binding protein (PTB). Huh-7 cells were transfected with pGEM (lanes 1), pGEM-3C (lanes 2) and pEXT7-HAV3C (lanes 3) and infected with vaccinia virus T7. Cell lysates were collected 24 h post-transfection and subjected to immunoblot using anti-3C, anti-poly(A)-binding protein and anti- PTB. As less $3C^{pro}$ was produced by pGEM-3C in comparison with pEXT7-HAV3C, cleavage of host proteins was more pronounced in lanes 3 when compared to lanes2.

reticulocyte lysate, and recombinant PTB produced in *E. coli* was substrate to cleavage-mediated *in vitro* by purified recombinant HAV $3C^{pro}$ (data not shown). Combined with its well-documented translation enhancing effect and binding specificity to stem-loop IIIa of the HAV IRES [6–8], the results strongly suggest that the inhibitory effect of HAV $3C^{pro}$ on HAV IRES translation is because of proteolytic cleavage of PTB.

## DISCUSSION

The expression level of the viral proteinase was found to substantially affect the detection of PTB cleavage products (see Fig. 4). Neither in HAV-infected cells nor in cells expressing the HAV replicon were PTB cleavage fragments detectable (not shown). A similar discrepancy was observed for PCBP, another ITAF that is essential for picornaviral translation and the molecular switching to RNA replication [9,23,24]. Whereas PCBP cleavage by recombinant HAV $3C^{pro}$ was clearly shown, PCBP-processing products were not apparent in extracts of HAV-infected cells [9]. Combined, our findings on HAV-3C-mediated cleavage of PCBP and PTB suggest that because of the protracted replication of HAV, very low quantities of $3C^{pro}$ are present in infected cells and cleavage of these host proteins is not discernible. This is in clear contrast to poliovirus whose highly efficient replication resulted in obvious cleavage of both PCBP and PTB [22,24].

The functional domains of PTB are four RNA recognition motifs that all bind short pyrimidine-rich sequences. By binding to different sites on the same RNA molecule, PTB can lead to distinctive RNA restructuring. Such conformational changes are thought to be critical in enabling the ribosomal recruitment in IRES-driven translation initiation. Our constructs do not include the 1–138 nt region of 5′NTR, in which a pyrimidine-rich-tract exists. PTB interacts with stem-loop IIIa of the HAV IRES that contains short polypyrimidine tracts [7]. These binding sites can be bridged by a single PTB molecule, which is an arrangement that favours a role for PTB as an RNA chaperone. It is likely that PTB stabilizes or alters the IRES structure to enable the recruitment of the ribosome and to position it correctly at the start codon.

For poliovirus, direct evidence was provided that PTB cleavage products inhibited IRES-dependent translation [22]. As outlined by the authors, it is possible that PTB fragments may interfere with the binding of intact PTB to poliovirus IRES or that cleaved PTB may no longer function as translational activator that facilitates the recruitment of translational machinery to the IRES element. Although not directly assessed here, it is assumed that suppression of HAV IRES translation is induced by similar mechanism(s). Moreover, in poliovirus-infected Hela cells, PTB cleavage fragments are redistributed to the cytoplasm [22]. As abundant quantities of PTB are present in the cytoplasm of Huh-7 cells used in our study [8], PTB redistribution might not be essential for the effect of PTB cleavage on HAV translation. Yet it is attractive to speculate that the PTB fragment(s) might have altered RNA-binding specificity. For poliovirus IRES translation, an attractive model was put forward for the participation of PTB and PCBP in the molecular switch from viral translation to RNA replication [22]. Supposedly, after viral 3C-mediated cleavage, PTB and PCBP lose their enhancing function. Once IRES translation is stalled, replication of the viral RNA consequently is turned on. Taken together with our earlier observations [9], HAV translation is inhibited indirectly by its own product, $3C^{pro}$, through the proteolytic cleavage of PCBP and PTB.

The HAV 3B and 3C proteins are 23 and 219 amino acids in length, respectively [25]. The 3B moiety was found to be essential for the 3AB interaction with 3CD [26]. It seems that 3BC was more suppressive than 3C in cap-independent translation. Further studies will reveal the 3B function in the interaction with PTB and 3BC. In conclusion, HAV proteinase 3C cleaved PTB and suppressed HAV IRES-dependent translation.

## ACKNOWLEDGEMENT

The authors thank Dr S.U. Emerson and Dr J. Miyazaki for pHM175 and pCXN2, respectively.

## STATEMENT OF PERSONAL INTERESTS

None of the authors have personal interests relevant to this research to declare.

## DECLARATION OF FUNDING INTERESTS

This work was supported by grants 21590829, 21590828 and 21390225 from the Japan Science and Technology Agency, Ministry of Education, Culture, Sports, Science and Technology, Japan (TK, FI and OY) and a grant from Chiba University Young Research-Oriented Faculty Member Development Program in Bioscience Areas (TK).

## REFERENCES

1 Martin A, Lemon SM. Hepatitis A virus: from discovery to vaccines. *Hepatology* 2006; 43(2 Suppl. 1): S164–S172.
2 Kanda T, Yokosuka O, Imazeki F *et al.* Amantadine inhibits hepatitis A virus internal ribosomal entry site-mediated translation in human hepatoma cells. *Biochem Biophys Res Commun* 2005; 331(2): 621–629.
3 Schultz DE, Honda M, Whetter LE *et al.* Mutations within the 5′ nontranslated RNA of cell culture adapted hepatitis A virus which enhance cap-independent translation in cultured African green monkey kidney cells. *J Virol* 1996; 70(2): 1041–1049.
4 Semler BL, Waterman ML. IRES-mediated pathways to polysomes: nuclear versus cytoplasmic routes. *Trends Microbiol* 2008; 16(1): 1–5.

5 Cordes S, Kusov Y, Heise T, Gauss-Müller V. La autoantigen suppresses IRES-dependent translation of the hepatitis A virus. *Biochem Biophys Res Commun* 2008; 368(4): 1014–1019.
6 Gosert R, Chang KH, Rijnbrand R *et al.* Transient expression of cellular polypyrimidine-tract binding protein stimulates cap-independent translation directed by both picornaviral and flaviviral internal ribosome entry sites in vivo. *Mol Cell Biol* 2000; 20(5): 1583–1595.
7 Schultz DE, Hardin CC, Lemon SM. Specific interaction of glyceraldehyde 3-phosphate dehydrogenase with the 5′-nontranslated RNA of hepatitis A virus. *J Biol Chem* 1996; 271(24): 14134–14142.
8 Yi M, Schultz DE, Lemon SM. Functional significance of the interaction of hepatitis A virus RNA with GAPDH: opposing effects of GAPDH and polypyrimidine tract binding protein on internal ribosome entry site function. *J Virol* 2000; 74(14): 6459–6468.
9 Zhang B, Seitz S, Kusov Y *et al.* RNA interaction and cleavage of poly(C)-binding protein 2 by hepatitis A virus protease. *Biochem Biophys Res Commun* 2007; 364(4): 725–730.
10 Sawicka K, Bushell M, Spriggs KA, Willis AE. Polypyrimidine-tract-binding protein: a multifunctional RNA-binding protein. *Biochem Soc Trans* 2008; 36(Pt 4): 641–647.
11 Kolupaeva VG, Hellen CU, Shatsky IN. Structural analysis of the interaction of the pyrimidine tract-binding protein with the internal ribosomal entry site of encephalomyocarditis virus and RNAs. *RNA* 1996; 2(12): 1199–1212.
12 Zhang B, Morace G, Gauss-Müller V, Kusov Y. Poly(A) binding protein, C-terminally truncated by the hepatitis A virus proteinase 3C, inhibits viral translation. *Nucleic Acids Res* 2007; 35(17): 5975–5984.
13 Gauss-Müller V, Kusov YY. Replication of a hepatitis A virus replicon detected by genetic recombination in vivo. *J Gen Virol* 2002; 83(Pt 9): 2183–2192.
14 Emerson SU, Lewis M, Govindarajan S *et al.* cDNA clone of hepatitis A virus encoding a virulent virus: induction of viral hepatitis by direct nucleic acid transfection of Marmosets. *J Virol* 1992; 66(11): 6649–6654.
15 Kanda T, Zhang B, Kusov Y *et al.* Suppression of hepatitis A virus genome translation and replication by siRNAs targeting the internal ribosomal entry site. *Biochem Biophys Res Commun* 2005; 330(4): 1217–1223.
16 Kanda T, Yokosuka O, Kato N *et al.* Hepatitis A virus VP3 may activate serum response element associated transcription. *Scand J Gastroenterol* 2003; 38(3): 307–313.
17 Niwa H, Yamamura K, Miyazaki J. Efficient selection for high-expression transfectants with a novel eukaryotic vector. *Gene* 1991; 108(2): 193–200.
18 Kanda T, Steele R, Ray R, Ray RB. Hepatitis C virus core protein augments androgen-receptor mediated signaling. *J Virol* 2008; 88(22): 11066–11072.
19 Chou MY, Underwood JG, Nikolic J *et al.* Multisite RNA binding and release of polypyrimidine tract binding protein during the regulation of c-src neural-specific splicing. *Mol Cell* 2000; 5(6): 949–957.
20 Kaminski A, Jackson RJ. The polypyrimidine tract binding protein (PTB) requirement for internal initiation of translation of cardiovirus RNAs is conditional rather than absolute. *RNA* 1998; 4(6): 626–638.
21 Kim YK, Jang SK. La protein is required for efficient translation driven by encephalomyocarditis virus internal ribosomal entry site. *J Gen Virol* 1999; 80(Pt 12): 3159–3166.
22 Back SH, Kim YK, Kim WJ *et al.* Translation of polioviral mRNA is inhibited by cleavage of polypyrimidine tract-binding proteins executed by polioviral $3C^{pro}$. *J Virol* 2002; 76(5): 2529–2542.
23 Gamarnik AV, Andino R. Switch from translation to RNA replication in a positive-stranded RNA virus. *Genes Dev* 1998; 12(15): 2293–2304.
24 Perera R, Daijogo S, Walter BL *et al.* Cellular protein modification by poliovirus: the two faces of poly(rC)-binding protein. *J Virol* 2007; 81(17): 8919–8932.
25 Totsuka A, Moritsugu Y. Hepatitis A virus proteins. *Intervirology* 1999; 42(2–3): 63–68.
26 Beneduce F, Ciervo A, Kusov Y *et al.* Mapping of protein domains of hepatitis A virus 3AB essential for interaction with 3CD and viral RNA. *Virol* 1999; 264(2): 410–421.

Research Article

EASL EUROPEAN ASSOCIATION FOR THE STUDY OF THE LIVER | JOURNAL OF HEPATOLOGY

# Association between mutations in the core region of hepatitis C virus genotype 1 and hepatocellular carcinoma development

Shingo Nakamoto, Fumio Imazeki*, Kenichi Fukai, Keiichi Fujiwara, Makoto Arai, Tatsuo Kanda, Yutaka Yonemitsu, Osamu Yokosuka

*Department of Medicine and Clinical Oncology, Graduate School of Medicine, Chiba University, 1-8-1 Inohana, Chuo-Ward, Chiba City, Chiba 260-8670, Japan*

**Background & Aims:** To determine whether amino acid mutations in the core region of hepatitis C virus (HCV) genotype 1 are associated with response to interferon (IFN) therapy and development of hepatocellular carcinoma (HCC).

**Methods:** We followed up 361 patients (median duration, 121 months), and IFN monotherapy was administered to 275 (76%) [sustained virological response (SVR) rate, 26.5%]. Using pretreatment sera, mutations at core residues 70 and 91 were analyzed [double wild (DW)-type amino acid pattern: arginine, residue 70; leucine, residue 91].

**Results:** A low aspartate aminotransferase (AST)/alanine aminotransferase (ALT) ratio and low HCV load were independently associated with SVR, but core mutations were not. During follow-up, 12 of 81 (14.8%) patients with the DW-type pattern and 52 of 216 (24.1%) patients with non-DW-type pattern developed HCC ($p = 0.06$, Breslow–Gehan–Wilcoxon test). Multivariate analysis with the Cox proportional-hazards model revealed the following independent risk factors for HCC: male gender [$p < 0.0001$; risk ratio (RR), 3.97], older age ($p < 0.05$; RR, 2.08), advanced fibrosis ($p < 0.0001$; RR, 5.75), absence of SVR ($p < 0.01$; RR, 10.0), high AST level ($p < 0.01$; RR, 2.08), high AST/ALT ratio ($p < 0.01$; RR, 2.21), and non-DW-type pattern ($p < 0.05$; RR, 1.96). In patients with F0–F2 fibrosis at entry, non-DW-type was likely to lead to cirrhosis ($p = 0.051$).

**Conclusions:** In HCV genotype 1 patients, HCC risk could be predicted by studying core mutations, response to IFN, and host factors like age, gender, and liver fibrosis.



Keywords: Hepatitis C virus; Core region; Hepatocellular carcinoma; Interferon; Sustained virological response.

*Received 30 April 2009; received in revised form 22 July 2009; accepted 4 August 2009; available online 23 October 2009*

* Corresponding author. Tel.: +81 43 226 2083; fax: +81 43 226 2088.

*E-mail address:* imazekif@faculty.chiba-u.jp (F. Imazeki).

*Abbreviations:* HCV, hepatitis C virus; IFN, interferon; HCC, hepatocellular carcinoma; SVR, sustained virological response; DW-type, double wild-type; RR, risk ratio; AST, aspartate aminotransferase; ALT, alanine aminotransferase; US, ultrasonography; CT, computed tomography; MRI, magnetic resonance imaging; PCR, polymerase chain reaction; OR, odds ratio.

## Introduction

Hepatitis C virus (HCV) infection is a global health problem and the number of chronic carriers worldwide is estimated at 170 million [1]. HCV causes chronic hepatitis, which may progress to liver cirrhosis and hepatocellular carcinoma (HCC); the speed of disease progression, though, varies among patients [2,3]. Age, gender, steatosis, liver fibrosis, and response to interferon (IFN) therapy are reported to be associated with disease progression and HCC development [4–7]. HCV has six major genotypes, of which genotype 1 is most common in Japan and reported to be associated with increased severity and progression of chronic liver disease [8,9]. HCV contributes to HCC by directly modulating the pathways promoting the malignant transformation of hepatocytes [10–13]. Studies on transgenic mice revealed that the HCV core protein has oncogenic potential [14], but other studies yielded conflicting results [15,16]. Recently, mutations at amino acids 70 and 91 in the core region were shown to predict virological response to therapy with IFN plus ribavirin and also HCC development [17–19]. However, few studies support these results, and hence, the clinical impact of core mutations on HCC development is still unclear. In order to determine the viral factors associated with HCC development, we performed a retrospective cohort study on 361 patients with chronic liver disease caused by HCV genotype 1 infection and analyzed the amino acids present at core residues 70 and 91. Additionally, we evaluated whether these mutations were associated with IFN treatment, cirrhosis development, or host factors like age and gender.

## Patients and methods

### *Study population*

We enrolled 361 consecutive HCV genotype 1-infected patients who had undergone liver biopsy between August 1986 and June 1998 at Chiba University Hospital. At the enrollment time, the absence of HCC was proven by abdominal ultrasonography (US), computed tomography (CT), or magnetic resonance imaging (MRI). All the patients tested positive for anti-HCV antibody, determined by second-generation enzyme-linked immunosorbent assay. Patients with chronic hepatitis B, autoimmune hepatitis, primary biliary cirrhosis, hemochromatosis, Wilson disease, or alcoholic liver disease were excluded, as were patients with a history of alcoholism, drug abuse, or IFN therapy. Written informed consent was obtained from all patients before performing liver biopsy.

**Table 1. Baseline characteristics of 361 hepatitis C (HCV) genotype 1-infected patients according to hepatocellular carcinoma (HCC) development.**

| Patients | $n = 361$ | HCC development | | |
|---|---|---|---|---|
| | | (+), $n = 82$ | (−), $n = 279$ | $p$ value |
| Gender (male/female) | 219/142 | 56/26 | 163/116 | 0.1 |
| Age (years) | 50.5 ± 12.2 | 56.8 ± 7.1 | 48.6 ± 12.7 | <0.0001 |
| BMI (kg/m$^2$) | 23.1 ± 2.9 | 23.1 ± 2.8 | 23.1 ± 3.3 | 0.82 |
| Staging of fibrosis (F0–1/F2/F3/F4) | 197/59/52/53 | 13/18/23/28 | 184/41/29/25 | <0.0001 |
| *IFN treatment and response* | | | | |
| SVR/non-SVR/non-IFN | 73/202/86 | 4/55/23 | 69/147/63 | 0.0004 |
| *Laboratory data* | | | | |
| AST (IU/L) | 87 ± 62 | 109 ± 59 | 80 ± 61 | 0.0001 |
| ALT (IU/L) | 125 ± 93 | 139 ± 80 | 121 ± 96 | 0.13 |
| AST/ALT | 0.75 ± 0.26 | 0.84 ± 0.28 | 0.73 ± 0.25 | 0.0003 |
| Platelets (10$^4$/mm$^3$) | 17.7 ± 6.7 | 13.0 ± 3.3 | 18.2 ± 6.9 | <0.0001 |
| Albumin (g/dL) | 4.2 ± 0.36 | 4.1 ± 0.39 | 4.3 ± 0.35 | <0.0001 |
| Total bilirubin (mg/dL) | 0.8 ± 0.6 | 0.9 ± 0.3 | 0.8 ± 0.6 | 0.39 |
| Core protein (pg/mL) | 201 ± 245 | 283 ± 273 | 177 ± 231 | 0.001 |
| *Amino acid pattern* | | | | |
| 70 Wild/non-wild/ND | 168/129/64 | 32/32/18 | 136/97/46 | 0.23* |
| 91 Wild/non-wild/ND | 139/158/64 | 28/36/18 | 111/122/46 | 0.58* |
| DW/non-DW/ND | 81/216/64 | 12/52/18 | 69/164/46 | 0.08* |

BMI, body mass index; DW, double wild (arginine at residue 70 and leucine at residue 91 in the core region); ND, not detected; ND cases were excluded.

The clinical backgrounds of the patients are shown in Table 1. The study population was predominantly male (59% men), and the mean age of the patients was 50.5 ± 12.2 years, with 15% patients having liver cirrhosis.

*Laboratory examination*

Serum samples were obtained and stored at −30 °C until analysis. We assumed that genotype 1 corresponds to group 1 when determining the HCV RNA genotypes by serologic grouping of serum antibodies [20]. The serum HCV load of the patients was determined at the time of liver biopsy, using the HCV core protein detection kit (Eiken Chemical, Tokyo, Japan; detection limit, 8 pg/mL) [21].

*Histopathological examination*

Percutaneous liver biopsy was performed, and specimens were histopathologically assessed as described previously [22]. According to the criteria of Desmet et al. [23], the staging of fibrosis was defined as F0 (no fibrosis), F1 (mild fibrosis), F2 (moderate fibrosis), F3 (severe fibrosis), and F4 (cirrhosis).

*Core nucleotide sequences*

HCV RNA was extracted from the serum samples obtained at the time of liver biopsy, and it was reverse-transcribed using SuperScript III reverse transcriptase (Invitrogen, Carlsbad, CA, USA). Nucleic acids were amplified by PCR with the

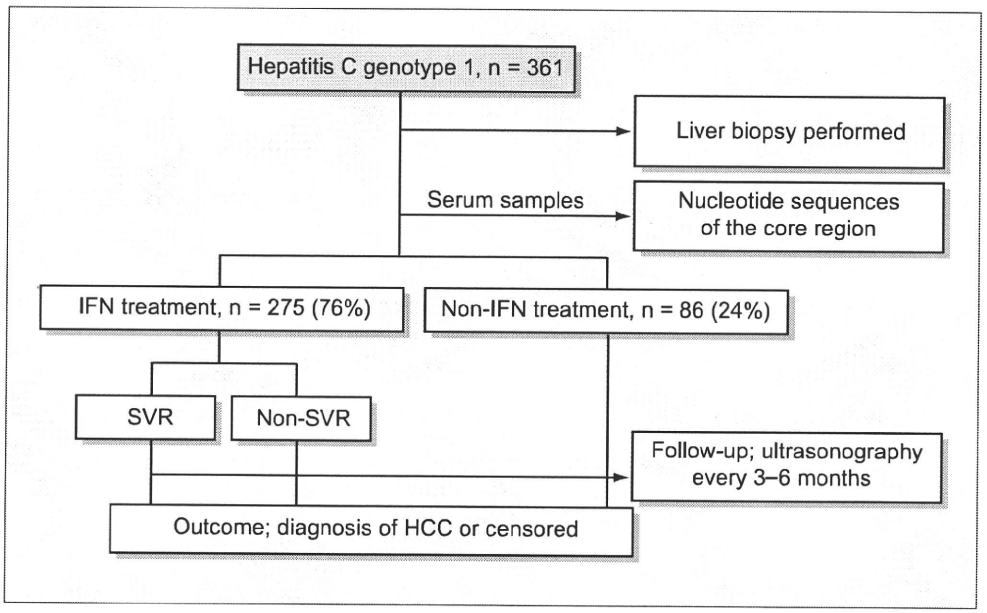


**Fig. 1. Clinical courses after enrollment and the evaluation methods.** IFN, interferon; SVR, sustained virological response; HCC, hepatocellular carcinoma. [This figure appears in colour on the web.]

HotStart Taq Master Mix kit (Qiagen, Hilden, Germany) and primers that have been previously described [24]. Polymerase chain reaction (PCR) was initiated with a denaturation step at 95 °C for 15 min, followed by 45 cycles at 94 °C for 1 min, 45 °C for 1 min, and 72 °C for 3 min, and subsequent extension for 7 min. PCR products were resolved by agarose gel electrophoresis, purified using the QIA quick PCR purification kit (Qiagen), and directly sequenced using a Big Dye Terminator v3.1 Cycle Sequencing kit (Applied Biosystems, Tokyo, Japan). The sequences were determined using an ABI PRISM 310 Genetic Analyzer (Applied Biosystems).

As described previously, the double wild-type (DW-type) amino acid pattern was defined as the presence of arginine at residue 70 (wild-type) and leucine at residue 91 (wild-type) [19].

*IFN treatment*

Depending on whether IFN was administered, the patients were divided into the IFN (76%) and non-IFN groups (24%) (Fig. 1). Patients who received IFN monotherapy during follow-up were divided into two subgroups: the sustained virological response (SVR) group, including patients who tested negative for HCV RNA at 24 weeks after completion of therapy, and non-SVR group (Fig. 1). Of the 275 patients in the IFN group, 73 (26.5%) achieved SVR.

*Follow-up and diagnosis of cirrhosis and HCC*

Clinical assessments were performed at least once every month during IFN treatment and every 3–6 months after the treatment. During follow-up, abdominal US was performed every 3–6 months to determine whether HCC had developed (Fig. 1). If necessary, additional procedures like CT, MRI, abdominal angiography, and US-guided tumor biopsy were performed to confirm HCC development. We also evaluated whether cirrhosis had developed in non-cirrhotic patients (F0–F2 stage). Cirrhosis was diagnosed according to the criteria of cirrhosis as described previously [25,26]. The follow-up period was the duration from the initial liver biopsy to HCC diagnosis or the last follow-up visit. For non-cirrhotic patients, this was the duration from the start point to cirrhosis diagnosis.

*Statistical analysis*

The $\chi^2$ test was used to compare categorical variables, and Student's $t$ test to compare continuous variables related to background characteristics among groups. Continuous variables were expressed as mean ± standard deviation. The cumulative incidence of HCC and cirrhosis was calculated using the Kaplan–Meier method and evaluated using the Breslow–Gehan–Wilcoxon test. Multivariate analysis was performed using the Cox proportional-hazards model or multiple logistic regression analysis. The Cochran–Armitage trend test was used for analyzing the association between the prevalence of mutation and subject age. Statistical significance was defined as $p < 0.05$.

## Results

*Cumulative HCC incidence*

During follow-up (median duration, 121 months; range, 8–257 months), 82 (22.7%) patients developed HCC [HCC group; 13 of 197 (6.6%) from F0–F1, 18 of 59 (30.5%) from F2, 23 of 52 (44.2%) from F3, and 28 of 53 (52.8%) from F4 stage at entry] and 279 (77.3%) did not (non-HCC group). The cumulative HCC incidence at 5, 10, and 15 years of follow-up was 9.5%, 22.9%, and 30.9%, respectively.

*Core nucleotide sequences*

The core nucleotide sequence was determined for 297 of 361 (82.3%) patients. In the entire patient group, the proportions of DW-type and non-DW-type patterns were 22% and 60%, respectively (Table 1).

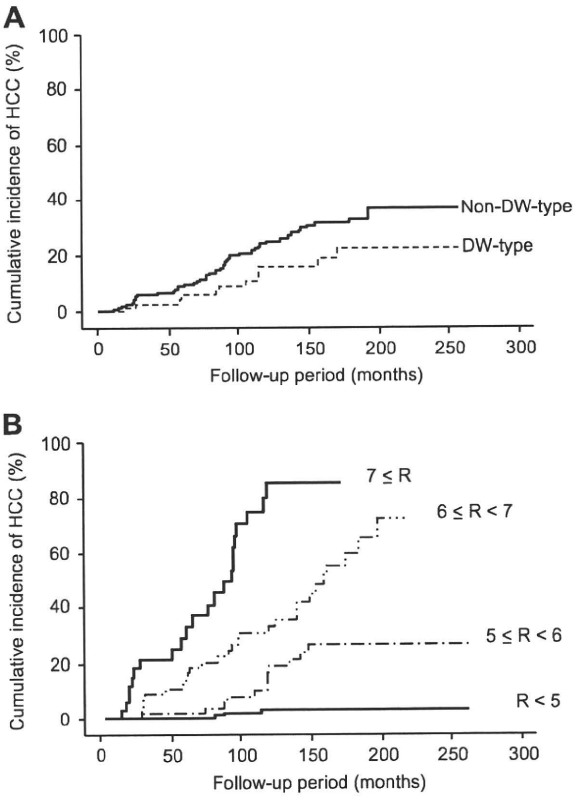


**Fig. 2. Cumulative incidence of hepatocellular carcinoma (HCC) in hepatitis C genotype 1-infected patients.** (A) Comparison between patients with double wild-type (DW-type: arginine, residue 70; leucine, residue 91) ($n = 81$) and non-DW-type ($n = 216$) amino acids in the core region ($p = 0.06$). (B) Comparison based on risk score ($R$) calculated using independent variables for HCC risk ($p < 0.0001$).

The core nucleotide sequence could not be determined for 64 patients because their samples showed significantly lower levels of the HCV core protein than those obtained from the 297 patients in whom the core sequence could be detected (119 vs. 217 pg/mL; $p = 0.0083$). There was no significant difference between the other variables shown in Table 1.

*Cumulative HCC incidence according to core amino acid mutations*

During follow-up, 12 of 81 (14.8%) patients with the DW-type pattern and 52 of 216 (24.1%) patients with the non-DW-type pattern developed HCC. Cumulative HCC incidence was 6.8% and 11% at 5 years, 19.1% and 27.7% at 10 years, and 26.6% and 38% at 15 years in the DW-type and non-DW-type groups, respectively. Cumulative HCC incidence in the DW-type group tended to be lower than that in the non-DW-type group ($p = 0.06$; Fig. 2A).

*Predictive factors associated with HCC development*

Potential predictive factors associated with HCC development are shown in Table 1. Univariate analysis revealed 10 parameters correlating with HCC development (Table 1). Multivariate analy-

**Table 2. Factors associated with hepatocellular carcinoma development in hepatitis C genotype 1-infected patients, identified by multivariate analysis using the Cox proportional-hazards model.**

| Factor* | Category | Risk ratio (95% CI) | *p* value |
|---|---|---|---|
| Gender | Male | 3.97 (2.05–7.63) | <0.0001 |
| | Female | 1.0 | |
| Age (years) | ⩾50 | 2.08 (1.01–4.33) | 0.049 |
| | <50 | 1.0 | |
| Staging of fibrosis | ⩾2 | 5.75 (2.68–12.35) | <0.0001 |
| | <2 | 1.0 | |
| IFN treatment and response | Absence of SVR | 10.0 (2.29–43.48) | 0.002 |
| | SVR | 1.0 | |
| AST (IU/L) | >90 | 2.08 (1.20–3.62) | 0.009 |
| | ⩽90 | 1.0 | |
| AST/ALT | ⩾0.8 | 2.21 (1.24–3.97) | 0.007 |
| | <0.8 | 1.0 | |
| Amino acid pattern | Non-DW | 1.96 (1.02–3.76) | 0.04 |
| | DW | 1.0 | |

CI, confidence intervals; DW, double wild (arginine at residue 70 and leucine at residue 91 in the core region).
*Significant factors are shown.

sis with the Cox proportional-hazards model showed that the following seven independent parameters were significantly associated with HCC development: male gender ($p < 0.0001$), age ⩾ 50 years ($p = 0.049$), fibrosis ⩾ F2 ($p < 0.0001$), absence of SVR ($p = 0.002$), aspartate aminotransferase (AST) level > 90 IU/L ($p = 0.009$), AST/alanine aminotransferase (ALT) ratio ⩾ 0.8 ($p < 0.007$), and non-DW-type pattern in the core region ($p = 0.04$) (Table 2).

*Prediction of HCC development based on risk score*

Using the predictive variables from the previous step (Table 2), the risk score ($R$) for HCC development was calculated from the beta coefficients derived from the Cox proportional-hazards model as follows: $R = 0.671 \times$ (non-DW-type) + $2.307 \times$ (absence of SVR) + $0.733 \times$ (AST > 90 IU/L) + $0.733 \times$ (age ⩾ 50 years) + $1.752 \times$ (staging of fibrosis ⩾ 2) + $1.378 \times$ (male) + $0.795 \times$ (AST/ALT ⩾ 0.8) (each variable: yes = 1, no = 0). Fig. 2B shows the cumulative HCC incidence of four subgroups categorized by risk score, and the RR of each group is shown in Table 3. The cumulative HCC incidence increased with the risk score: from highest to lowest it was 84.7%, 35.1%, 18.5%, and 3.0% at 10 years.

*Cumulative HCC incidence according to IFN treatment and response*

During follow-up, 4 (5.5%) patients in the SVR, 55 (27.2%) in the non-SVR, and 23 (26.7%) in the non-IFN groups developed HCC; cumulative HCC incidence was 0%, 11.3%, and 13.2%, respectively, at 5 years; 7.8%, 25.6%, and 27.3%, respectively, at 10 years; and 7.8%, 36.5%, and 35.5%, respectively, at 15 years. Moreover, cumulative HCC incidence was significantly lower in the SVR group than other groups ($p < 0.001$; Fig. 3).

**Table 3. Relative risk of HCC development based on risk score, using the Cox proportional-hazards model.**

| Score ($R$) | Risk ratio (95% CI) | *p* value |
|---|---|---|
| $R < 5$ | 1 | |
| $5 \leqslant R < 6$ | 9.22 (2.60–32.7) | 0.0006 |
| $6 \leqslant R < 7$ | 26.9 (8.15–89.0) | <0.0001 |
| $7 \leqslant R$ | 88.3 (25.8–302) | <0.0001 |

CI, confidence intervals.

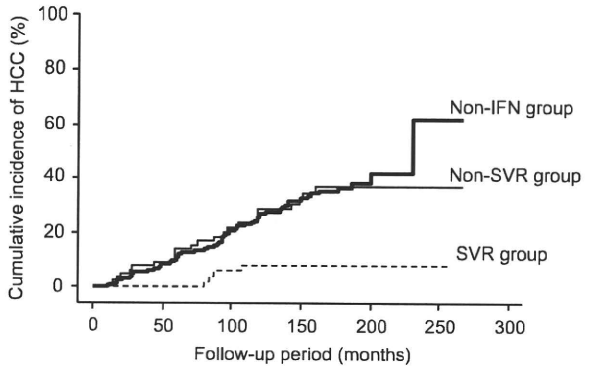


**Fig. 3. Cumulative incidence of hepatocellular carcinoma (HCC).** Comparison between the sustained virological response (SVR) ($n = 73$), non-SVR ($n = 202$), and non-interferon (IFN) ($n = 86$) groups ($p = 0.002$).

*Analysis of SVR-associated factors*

Compared to those in the non-IFN group, patients in the IFN group were younger (49 years vs. 54 years, $p = 0.003$), had higher aminotransferase levels (AST, 93 vs. 68 IU/L, $p = 0.001$; ALT, 137 vs. 87 IU/L, $p < 0.0001$) and lower core protein levels (183 vs. 263 pg/mL, $p = 0.01$). Table 4 shows baseline characteristics of patients according to interferon response. Univariate analysis revealed six SVR-associated parameters, whereas multiple logistic regression analysis revealed two independent significant predictors of SVR: AST/ALT ratio of <0.8 [$p = 0.005$; odds ratio (OR), 3.09; 95% confidence interval (CI), 1.40–6.82] and core protein level of <200 pg/mL [$p < 0.0001$; OR, 70.94; 95% CI, 9.56–526.2]. However, both univariate ($p = 0.64$) and multivariate analyses (data not shown) showed that the DW-type pattern in the core region was not associated with SVR.

**Table 4. Baseline characteristics of patients according to interferon response.**

| Nature of the Regime | SVR $n = 73$ | Non-SVR $n = 202$ | *p* value |
|---|---|---|---|
| Gender (Male/Female) | 47/26 | 126/76 | 0.76 |
| Age (years) | 46.6 ± 13.3 | 50.5 ± 11.5 | 0.02 |
| BMI (kg/m$^2$) | 22.7 ± 2.8 | 23.2 ± 3.0 | 0.24 |
| Staging of fibrosis: (F0-1/F2/F3/F4) | 45/12/9/7 | 104/34/34/30 | 0.42 |
| Laboratory data | | | |
| AST (IU/L) | 79 ± 56 | 97 ± 69 | 0.048 |
| ALT (IU/L) | 132 ± 92 | 139±100 | 0.60 |
| AST/ALT | 0.65 ± 0.22 | 0.75 ± 0.27 | 0.003 |
| Platelets ($10^4$/mm$^3$) | 18.6 ± 6.7 | 16.7 ± 6.1 | 0.03 |
| Albumin (g/dL) | 4.3 ± 0.3 | 4.2 ± 0.4 | 0.06 |
| Total bilirubin (mg/dL) | 0.7 ± 0.4 | 0.8 ± 0.4 | 0.02 |
| Core protein (pg/mL) | 31 ± 50 | 234 ± 226 | <0.0001 |
| Amino acid pattern | | | |
| 70 Wild/Non-wild/ND | 35/21/17 | 89/74/39 | 0.30 |
| 91 Wild/Non-wild/ND | 24/32/17 | 76/87/39 | 0.62 |
| DW/Non-DW/ND | 14/42/17 | 46/117/39 | 0.64 |

BMI, body mass index; DW, double wild (arginine at residue 70 and leucine at residue 91 in the core region); ND, not detected.

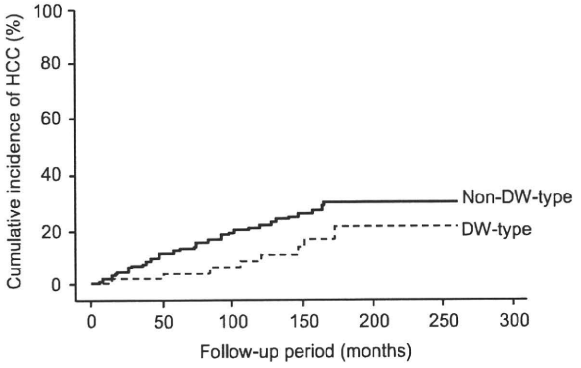


**Fig. 4. Cumulative incidence of cirrhosis in non-cirrhotic patients (F0–F2).** Comparison between patients with double wild-type (DW-type: arginine, residue 70; leucine, residue 91) ($n = 81$) and non-DW-type ($n = 216$) amino acids in the core region ($p = 0.051$).

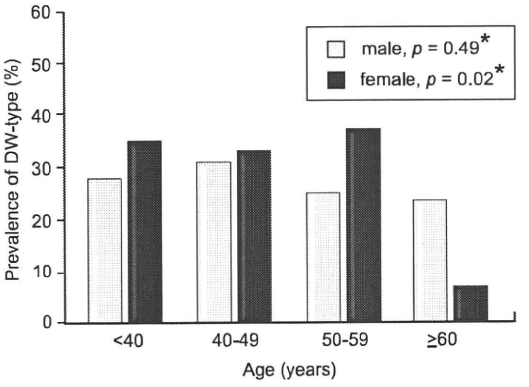


**Fig. 5. Prevalence of double wild-type (DW-type: arginine, residue 70; leucine, residue 91) amino acids in the hepatitis C core region according to age and gender.** *By the Cochran-Armitage trend test.

*Cumulative cirrhosis incidence for non-cirrhotic patients (F0–F2)*

Of the 256 non-cirrhotic patients (197 from F0–F1, 59 from F2), 50 (19.5%) developed cirrhosis (cirrhosis group) and 206 (80.5%) did not (non-cirrhosis group). The cumulative cirrhosis incidence at 5, 10, and 15 years of follow-up was 9.7%, 18.2%, and 26.4%, respectively. The HCC incidence was higher in the cirrhosis group [23/50 (46%)] than the non-cirrhosis group [8/206 (3.9%); $p < 0.0001$]. In the entire population, 71 of 82 (86.6%) patients who developed HCC had underlying cirrhosis and 11 (13.4%) did not, when HCC was detected ($p < 0.0001$).

*Cumulative cirrhosis incidence according to the amino acid pattern in the core region for F0–F2 patients*

The cumulative cirrhosis incidence tended to be higher in the non-DW-type group than the DW-type group (11.9% and 3.6% at 5 years, 21.5% and 10.4% at 10 years, and 29.7% and 20.7% at 15 years of follow-up, respectively; $p = 0.051$; Fig. 4).

*Analysis of factors associated with cirrhosis development in F0–F2 patients*

We analyzed the factors associated with cirrhosis development in patients with F0–F2 fibrosis at enrollment. Univariate analysis revealed nine parameters correlating with cirrhosis development: male gender ($p = 0.04$), older age ($p < 0.0001$), advanced fibrosis ($p < 0.0001$), absence of SVR ($p < 0.0001$), high AST level ($p < 0.0001$), high ALT level ($p = 0.01$), high AST/ALT ratio ($p = 0.001$), low platelet count ($p = 0.0009$), and high core protein level ($p = 0.02$). Multivariate analysis, including analysis of the amino acid pattern in the core region with the Cox proportional-hazards model, showed that the following three independent parameters were significantly associated with cirrhosis development: male gender ($p = 0.004$), fibrosis = F2 ($p = 0.004$), and absence of SVR ($p = 0.02$). Meanwhile, the presence of the non-DW-type pattern in the core region tended to lead to cirrhosis development (RR, 2.13; 95% CI, 0.93–4.91; $p = 0.07$).

*Analysis of factors associated with mutations at core residues 70 and 91*

Eighty-one patients with the DW-type pattern at core residues 70 and 91, who were at low risk for HCC, tended to be younger than the 216 patients with the non-DW-type pattern, who were at high risk for HCC (48.4 ± 11.8 years vs. 51.1 ± 11.8 years, respectively; $p = 0.08$). Separate analysis of men and women (Fig. 5) showed that the DW-type pattern was rare in women aged 60 years or above ($p = 0.02$).

Consistent with these results, HCC incidence was the same in men and women aged 60 or above (19% vs. 10% at 5 years and 32% vs. 38% at 10 years of follow-up, respectively; $p = 0.89$); however, in patients aged less than 60 years, HCC incidence was lower in women than in men (4% vs. 11% at 5 years and 15% vs. 22% at 10 years of follow-up, respectively; $p = 0.03$).

## Discussion

Male gender, older age, advanced-stage fibrosis, and no IFN treatment are reported as important predictors of HCC development in chronic hepatitis C patients [4–7]. Viral factors associated with HCC development were also reported [27–29]. Several studies showed that mutations in the core protein are associated with HCC among HCV genotype 1b-infected patients, but the results varied between studies [18,30,31]. Consistent with a report by Akuta et al. [18], we showed that the presence of the non-DW-type pattern at core residues 70 and 91 is an independent risk factor for HCC development. Akuta et al. [18] studied 313 chronic hepatitis C patients who received IFN therapy (101 were excluded), and found that non-DW-type was an independent risk factor for HCC development (RR, 5.92; 95% CI, 1.58–22.2; $p = 0.008$) by using the Cox proportional-hazards model, and its correlation with HCC risk was stronger than that found in our study (RR, 1.96; 95% CI, 1.02–3.76; $p = 0.04$). We analyzed cirrhotic patients (14.7% of total population), most of whom developed HCC, and also non-cirrhotic patients, and found that the non-DW-type was still an independent risk factor for HCC development (RR, 2.90; 95% CI, 1.11–7.61; $p = 0.03$). Furthermore, we

found that the non-DW-type in patients with F0–F2 fibrosis was likely to lead to cirrhosis, diagnosed by US ($p = 0.051$). Moreover, the non-DW-type in patients with F0–F3 fibrosis was significantly associated with cirrhosis development ($p = 0.007$, data not shown). These results suggest that the non-DW-type may affect HCC development by accelerating cirrhosis development; however, prospective studies of histological findings are needed to confirm this.

It is unclear why the amino acids at residues 70 and 91 affect HCC development. The core protein cooperates with the Ras oncogene and transforms primary rat embryo fibroblasts into the tumorigenic phenotype [10]. The HCV core protein (residues 25–91) also interacts with the heterogeneous nuclear ribonucleoprotein K, which stimulates the c-myc promoter, downstream of the Wnt/beta-catenin signal [11]. Pavio et al. reported that the HCV core (residues 59–126, residues at 70 and 91 were non-wild-type) interacts with Smad3 and inhibits the TGF-beta pathway, important in apoptosis [12]. Mutations in the clustering variable regions (residues 39–76) are often seen in HCC patients [30], and mutations in the *N*-myristoylation sites (e.g., residue 91) in the core region, are associated with growth control and virus replication [31]. Delhem et al. have shown that the core protein with non-wild-type amino acids at residues 70 and 91 obtained from a HCC patient binds and activates PKR, which might cause carcinogenesis [13]. It was reported that the presence of a non-wild-type amino acid at residue 91 enhances internal initiation of HCV protein synthesis, leading to the expression of a core isoform, which may interact with viral and cellular components [32]. These results suggest that residues 70 and 91 themselves or via interactions with adjacent amino acids may be involved in HCC development; however, further studies are needed to evaluate the effect of core mutations on HCC development.

The presence of the DW-type pattern in the core region is also reportedly a predictor of the virological response to therapy with peginterferon and ribavirin [19]. With this therapy, an SVR of approximately 50% could be achieved by HCV genotype 1-infected patients having high viral load. We found the absence of an SVR and the non-DW-type pattern to be predictors of HCC development; however, the non-DW-type pattern was not a predictor of the absence of an SVR. This may be partly because we used IFN monotherapy without ribavirin, with which the SVR rate (26.5% in our study) was lower than that with peginterferon plus ribavirin [33,34]. Therefore, we believe that combination therapy, rather than IFN monotherapy, would more efficiently eradicate HCV with the DW-type pattern in the core region; however, further studies are required to test this hypothesis. Our current focus is on a prospective study to examine the association between core mutations and the outcome of combination treatment with peginterferon plus ribavirin.

Our study revealed that the DW-type pattern, associated with a low HCC risk, was rare in women aged 60 years or above. This may explain why HCC incidence in women was as high as that in men. The underlying mechanisms by which age or gender influence core-region mutations are unknown. In previous studies, a mutation at residue 70 was correlated with virological response to therapy with IFN plus ribavirin [17] and with AFP levels [35] in HCV genotype 1b-infected patients without HCC. Further follow-up studies must examine whether a mutation occurs in the wild-type amino acid.

We investigated two specific amino acid mutations in the HCV core region by direct sequencing. The HCV core sequence can be easily amplified using PCR because of its conservative nature and analysis of only two amino acid positions is timesaving; therefore, this method might be feasible for identifying predictive markers for HCC. A specific PCR method for detecting these mutations was reported [36]. Furthermore, we developed a rapid and sensitive real-time PCR method for quantitatively detecting these mutations [37]. We hope this method can be used to detect HCV sequences in case of a low viral load, and believe that it will be more useful for predicting HCC.

In conclusion, HCC risk could be predicted by studying mutations in the HCV core region, response to IFN, and host factors like age, gender, and liver fibrosis in HCV genotype 1-infected patients. These mutations might be involved in an oncogenic mechanism leading to HCC development in chronic HCV patients.

## Financial disclosures

All authors have nothing to disclose.

## Acknowledgements

The authors who have taken part in this study declared that they do not have anything to disclose regarding funding from industries or conflict of interest with respect to this manuscript.

## References

[1] Seeff LB. Natural history of chronic hepatitis C. Hepatology 2002;36:S35–S46.
[2] Saito I, Miyamura T, Ohbayashi A, Harada H, Katayama T, Kikuchi S, et al. Hepatitis C virus infection is associated with the development of hepatocellular carcinoma. Proc Natl Acad Sci USA 1990;87:6547–6549.
[3] Poynard T, Bedossa P, Opolon P. Natural history of liver fibrosis progression in patients with chronic hepatitis C. The OBSVIRC, METAVIR, CLINIVIR, and DOSVIRC groups. Lancet 1997;349:825–832.
[4] Yoshida H, Shiratori Y, Moriyama M, Arakawa Y, Ide T, Sata M, et al. Interferon therapy reduces the risk for hepatocellular carcinoma: national surveillance program of cirrhotic and noncirrhotic patients with chronic hepatitis C in Japan. IHIT Study group. Inhibition of hepatocarcinogenesis by interferon therapy. Ann Intern Med 1999;131:174–181.
[5] Freeman AJ, Dore GJ, Law MG, Thorpe M, Von Overbeck J, Lloyd AR, et al. Estimating progression to cirrhosis in chronic hepatitis C virus infection. Hepatology 2001;34:809–816.
[6] Fartoux L, Chazouilleres O, Wendum D, Poupon R, Serfaty L. Impact of steatosis on progression of fibrosis in patients with mild hepatitis C. Hepatology 2005;41:82–87.
[7] Lok AS, Seeff LB, Morgan TR, di Bisceglie AM, Sterling RK, Curto TM, et al. Incidence of hepatocellular carcinoma and associated risk factors in hepatitis C-related advanced liver disease. Gastroenterology 2009;136:138–148.
[8] Simmonds P, Bukh J, Combet C, Deleage G, Enomoto N, Feinstone S, et al. Consensus proposals for a unified system of nomenclature of hepatitis C virus genotypes. Hepatology 2005;42:962–973.
[9] Ikeda K, Kobayashi M, Someya T, Saitoh S, Tsubota A, Akuta N, et al. Influence of hepatitis C virus subtype on hepatocellular carcinogenesis: a multivariate analysis of a retrospective cohort of 593 patients with cirrhosis. Intervirology 2002;45:71–78.
[10] Ray RB, Lagging LM, Meyer K, Ray R. Hepatitis C virus core protein cooperates with ras and transforms primary rat embryo fibroblasts to tumorigenic phenotype. J Virol 1996;70:4438–4443.
[11] Hsieh TY, Matsumoto M, Chou HC, Schneider R, Hwang SB, Lee AS, et al. Hepatitis C virus core protein interacts with heterogeneous nuclear ribonucleoprotein K. J Biol Chem 1998;273:17651–17659.
[12] Pavio N, Battaglia S, Boucreux D, Arnulf B, Sobesky R, Hermine O, et al. Hepatitis C virus core variants isolated from liver tumor but not from

adjacent non-tumor tissue interact with Smad3 and inhibit the TGF-beta pathway. Oncogene 2005;24:6119–6132.
[13] Delhem N, Sabile A, Gajardo R, Podevin P, Abadie A, Blaton MA, et al. Activation of the interferon-inducible protein kinase PKR by hepatocellular carcinoma derived-hepatitis C virus core protein. Oncogene 2001;20:5836–5845.
[14] Moriya K, Fujie H, Shintani Y, Yotsuyanagi H, Tsutsumi T, Ishibashi K, et al. The core protein of hepatitis C virus induces hepatocellular carcinoma in transgenic mice. Nat Med 1998;4:1065–1067.
[15] Perlemuter G, Sabile A, Letteron P, Vona G, Topilco A, Chretien Y, et al. Hepatitis C virus core protein inhibits microsomal triglyceride transfer protein activity and very low density lipoprotein secretion: a model of viral-related steatosis. FASEB J 2002;16:185–194.
[16] Honda A, Hatano M, Kohara M, Arai Y, Hartatik T, Moriyama T, et al. HCV-core protein accelerates recovery from the insensitivity of liver cells to Fas-mediated apoptosis induced by an injection of anti-Fas antibody in mice. J Hepatol 2000;33:440–447.
[17] Donlin MJ, Cannon NA, Yao E, Li J, Wahed A, Taylor MW, et al. Pretreatment sequence diversity differences in the full-length hepatitis C virus open reading frame correlate with early response to therapy. J Virol 2007;81:8211–8224.
[18] Akuta N, Suzuki F, Kawamura Y, Yatsuji H, Sezaki H, Suzuki Y, et al. Amino acid substitutions in the hepatitis C virus core region are the important predictor of hepatocarcinogenesis. Hepatology 2007;46:1357–1364.
[19] Akuta N, Suzuki F, Kawamura Y, Yatsuji H, Sezaki H, Suzuki Y, et al. Predictive factors of early and sustained responses to peginterferon plus ribavirin combination therapy in Japanese patients infected with hepatitis C virus genotype 1b: amino acid substitutions in the core region and low-density lipoprotein cholesterol levels. J Hepatol 2007;46: 403–410.
[20] Tanaka T, Tsukiyama-Kohara K, Yamaguchi K, Yagi S, Tanaka S, Hasegawa A, et al. Significance of specific antibody assay for genotyping of hepatitis C virus. Hepatology 1994;19:1347–1353.
[21] Tanaka E, Kiyosawa K, Matsumoto A, Kashiwakuma T, Hasegawa A, Mori H, et al. Serum levels of hepatitis C virus core protein in patients with chronic hepatitis C treated with interferon alfa. Hepatology 1996;23:1330–1333.
[22] Imazeki F, Yokosuka O, Fukai K, Saisho H. Favorable prognosis of chronic hepatitis C after interferon therapy by long-term cohort study. Hepatology 2003;38:493–502.
[23] Desmet VJ, Gerber M, Hoofnagle JH, Manns M, Scheuer PJ. Classification of chronic hepatitis: diagnosis, grading and staging. Hepatology 1994;19:1513–1520.
[24] Enomoto N, Sakuma I, Asahina Y, Kurosaki M, Murakami T, Yamamoto C, et al. Comparison of full-length sequences of interferon-sensitive and resistant hepatitis C virus 1b. Sensitivity to interferon is conferred by amino acid substitutions in the NS5A region. J Clin Invest 1995;96:224–230.
[25] Simonovsky V. The diagnosis of cirrhosis by high resolution ultrasound of the liver surface. Br J Radiol 1999;72:29–34.
[26] Kudo M, Zheng RQ, Kim SR, Okabe Y, Osaki Y, Iijima H, et al. Diagnostic accuracy of imaging for liver cirrhosis compared to histologically proven liver cirrhosis. A multicenter collaborative study. Intervirology 2008;51:17–26.
[27] Ogat S, Ku Y, Yoon S, Makino S, Nagano-Fujii M, Hotta H. Correlation between secondary structure of an amino-terminal portion of the nonstructural protein 3 (NS3) of hepatitis C virus and development of hepatocellular carcinoma. Microbiol Immunol 2002;46:549–554.
[28] Gimenez-Barcons M, Franco S, Suarez Y, Forns X, Ampurdanes S, Puig-Basagoiti F, et al. High amino acid variability within the NS5A of hepatitis C virus (HCV) is associated with hepatocellular carcinoma in patients with HCV-1b-related cirrhosis. Hepatology 2001;34:158–167.
[29] De Mitri MS, Morsica G, Cassini R, Bagaglio S, Zoli M, Alberti A, et al. Prevalence of wild-type in NS5A-PKR protein kinase binding domain in HCV-related hepatocellular carcinoma. J Hepatol 2002;36:116–122.
[30] Shimizu I, Yao DF, Horie C, Yasuda M, Shiba M, Horie T, et al. Mutations in a hydrophilic part of the core gene of hepatitis C virus in patients with hepatocellular carcinoma in China. J Gastroenterol 1997;32:47–55.
[31] Horie T, Shimizu I, Horie C, Yogita S, Tashiro S, Ito S. Mutations of the core gene sequence of hepatitis C virus isolated from liver tissues with hepatocellular carcinoma. Hepatol Res 1999;13:240–251.
[32] Eng FJ, Walewski JL, Klepper AL, Fishman SL, Desai SM, McMullan LK, et al. Internal initiation stimulates production of p8 minicore, a member of a newly discovered family of hepatitis C virus core protein isoforms. J Virol 2009;83:3104–3114.
[33] Schalm SW, Hansen BE, Chemello L, Bellobuono A, Brouwer JT, Weiland O, et al. Ribavirin enhances the efficacy but not the adverse effects of interferon in chronic hepatitis C. Meta-analysis of individual patient data from European centers. J Hepatol 1997;26:961–966.
[34] Mangi A, Villani MR, Minerva N, Leandro G, Bacca D, Cela M, et al. Efficacy of 5 MU of interferon in combination with ribavirin for naive patients with chronic hepatitis C virus: a randomized controlled trial. J Hepatol 2001;34:441–446.
[35] Akuta N, Suzuki F, Kawamura Y, Yatsuji H, Sezaki H, Suzuki Y, et al. Substitution of amino acid 70 in the hepatitis C virus core region of genotype 1b is an important predictor of elevated alpha-fetoprotein in patients without hepatocellular carcinoma. J Med Virol 2008;80:1354–1362.
[36] Okamoto K, Akuta N, Kumada H, Kobayashi M, Matsuo Y, Tazawa H. A nucleotide sequence variation detection system for the core region of hepatitis C virus-1b. J Virol Methods 2007;141:1–6.
[37] Nakamoto S, Kanda T, Yonemitsu Y, Arai M, Fujiwara K, Fukai K, et al. Quantification of hepatitis C amino acid substitutions 70 and 91 in the core coding region by real-time amplification refractory mutation system reverse transcription-polymerase chain reaction. Scand J Gastroenterol 2009:1–6.

European Journal of Radiology 75 (2010) e102–e106

Contents lists available at ScienceDirect

European Journal of Radiology

journal homepage: www.elsevier.com/locate/ejrad

# Changes in tumor vascularity precede microbubble contrast accumulation deficit in the process of dedifferentiation of hepatocellular carcinoma

Hitoshi Maruyama*, Masanori Takahashi, Hiroyuki Ishibashi, Shinichiro Okabe, Masaharu Yoshikawa, Osamu Yokosuka

*Department of Medicine and Clinical Oncology, Chiba University Graduate School of Medicine 1-8-1, Inohana, Chuou-ku, Chiba 260-8670, Japan*

ARTICLE INFO

*Article history:*
Received 19 June 2009
Received in revised form 22 August 2009
Accepted 25 August 2009

*Keywords:*
Ultrasound
Hepatocellular carcinoma
Contrast agent
Sonazoid
Nodule-in-nodule

ABSTRACT

*Purpose:* To elucidate the changes in tumor vascularity and microbubble accumulation on contrast-enhanced sonograms, in relation to the dedifferentiation of hepatocellular carcinoma (HCC).
*Materials and methods:* This prospective study enrolled 10 patients with histologically proven HCC (14.4–39.0 mm, 26.1 ± 7.4) showing nodule-in-nodule appearance upon contrast-enhanced computed tomography. Contrast-enhanced ultrasound was performed by harmonic imaging under a low mechanical index (0.22–0.25) during the vascular phase (agent injection to 1 min) and late phase (15 min) following the injection of Sonazoid™ (0.0075 ml/kg). Contrast enhancement in the inner and outer nodules was assessed in comparison with that in adjacent liver parenchyma as hyper-, iso-, or hypo-enhanced.
*Results:* Vascular-phase enhancement of all 10 inner nodules was hyper-enhanced, and that of outer nodules was hyper-enhanced in 3, iso-enhanced in 2, and hypo-enhanced in 5. Late-phase enhancement of inner nodules was hypo-enhanced in 8 and iso-enhanced in 2. Furthermore, late-phase enhancement of outer nodules was iso-enhanced in the 7 lesions that showed iso- or hypo-enhancement in the vascular phase, and hypo-enhanced in the 3 with hyper-enhancement in the vascular phase. Late-phase hypo-enhancement was significantly more frequent in the nodules showing early-phase hyper-enhancement (11/13) than in the nodules showing early-phase iso- or hypo-enhancement (0/7) in both the inner and outer nodules.
*Conclusion:* Dedifferentiation of HCC may be accompanied by changes in tumor vascularity prior to a reduction in microbubble accumulation. Observation of the vascular phase may be more useful than late-phase imaging for the early recognition of HCC dedifferentiation when using contrast-enhanced ultrasound with Sonazoid.



## 1. Introduction

Hepatocellular carcinoma (HCC) is one of the most common malignancies, and its incidence is increasing worldwide, especially in the eastern part of Asia [1,2]. The diagnosis of HCC is an issue of critical importance, in part because the prognosis of patients with cirrhosis depends to a large extent on the occurrence and progression of this neoplasm. Considering the limitations of tumor markers such as alpha fetoprotein (AFP) for HCC surveillance, it is necessary to have easy access to imaging examinations for cirrhotic patients [3,4].

Intra-tumor vascularity changes during the multistep process of carcinogenesis in HCC, including the presence of numerous tumor vessels, as well as a paucity of Kupffer cells comprise the well-known pathological appearance that is characteristic of HCC [5–7]. However, some well-differentiated HCCs have a hypo- or iso-vascular appearance, along with Kupffer cells distributed within the tumor nodule [6,7]. The relationship between the changes in tumor vascularity and Kupffer cell distribution, in accordance with the dedifferentiation process of HCC, has not been fully addressed in previous studies.

Contrast-enhanced ultrasound (US) has become popular as a non-invasive diagnostic tool for assessing focal hepatic lesions, due to the recent advances in digital technology incorporated into US equipment [8–10]. Microbubble contrast agents can be divided into two classes based on whether they do or do not accumulate in the liver, and both Levovist® (Schering, Berlin, Germany) and Sonazoid™ (GE Healthcare, Oslo, Norway) are classified as the former. They provide images of static microbubbles, which appear to demonstrate the function of the reticuloendothelial system such as phagocytosis by Kupffer cells, as well as imaging dynamic microbubbles that depict the hemodynamic circulation [11–14]. Therefore, contrast-enhanced US with these microbubble

* Corresponding author. Tel.: +81 43 2262083; fax: +81 43 2262088.
*E-mail addresses:* maru-cib@umin.ac.jp (H. Maruyama), machat@aa.pial.jp (M. Takahashi), bashiish@yahoo.co.jp (H. Ishibashi), okabeshin1966@yahoo.co.jp (S. Okabe), yoshikawa@faculty.chiba-u.jp (M. Yoshikawa), yokosukao@faculty.chiba-u.jp (O. Yokosuka).

0720-048X/$ – see front matter © 2009 Elsevier Ireland Ltd. All rights reserved.
doi:10.1016/j.ejrad.2009.08.017

contrast agents may reveal both tumor vascularity and Kupffer cell distribution in HCC lesions.

The nodule-in-nodule appearance of HCCs is a pattern that reflects cell dedifferentiation, because tumor elements with varying degrees of differentiation coexist in a single mass [15–20]. Assessment of contrast-enhanced US findings in HCCs with nodule-in-nodule appearance may reveal the dedifferentiation-related changes involved with tumor neovascularity and Kupffer cell distribution in these HCC lesions [21]. Against this background, we examined differences in contrast enhancement between the inner and outer nodules in HCC lesions having a nodule-in-nodule appearance. The purpose of this study was to elucidate the changes in tumor vascularity and microbubble accumulation exhibited on contrast-enhanced sonograms, in relation to the dedifferentiation of HCC.

## 2. Patients and methods

### 2.1. Patients

During the period from July 2007 to February 2009, a prospective study approved by the Ethics Committee of Chiba University Hospital, Chiba, Japan, was performed to examine Sonazoid-induced enhancement on sonograms of patients with HCC, after obtaining their informed written consent. A total of 513 patients with HCC underwent both contrast-enhanced computed tomography (CT) and contrast-enhanced US examination during this time period. There were 10 consecutive patients with HCC showing a nodule-in-nodule appearance upon contrast-enhanced CT, specifically, an inner nodule with hypervascularity and an outer nodule with a hypo-, iso-, or slightly hypervascular appearance on the images in the hepatic artery-dominant phase. The study enrolled these 10 cirrhotic patients as subjects, with all their HCC lesions proven histologically. The study patients consisted of 5 males and 5 females, with a mean age ± standard deviation (SD) of 67.3 ± 8.9 years (range 45–78 years). The diagnosis of liver cirrhosis was based on imaging findings, along with clinical symptoms and biochemistry results in all 10 patients; 9 of the patients were positive for hepatitis C virus antibody, and one patient was positive for hepatitis B virus surface antigen.

Each patient had one HCC tumor mass with a nodule-in-nodule appearance and a maximum diameter ranging from 14.4 to 39.0 mm (mean 26.1 ± 7.4 mm) on the sonogram. The serum AFP level ranged from 3.4 to 1266.1 ng/ml, with normal values (<20 ng/ml) found in 6 patients and abnormal values in 4 patients. No patients had egg allergy, which is a contraindication to the use of Sonazoid.

### 2.2. US examination

US examination was performed using the SSA-790A system (Aplio XG; Toshiba Medical Systems, Tokyo, Japan) with a 3.75-MHz convex probe. All patients underwent US examination after a fast of more than 4 h. At first, non-contrast grey-scale US (tissue harmonic imaging, 2.5/5.0 MHz, 14–27 Hz) was performed to observe the tumor appearance, to measure the diameters of the inner and outer nodules, and to select the scan plane allowing the most stable observation for contrast-enhanced US. Subsequently, color Doppler US was used to check for the presence or absence of vascular abnormality, such as arterio-portal communication, portal vein thrombosis, and/or portal vein tumor thrombosis. Next, the settings of the US system were changed for contrast-enhanced US, that is, to use the pulse subtraction harmonic imaging mode with a mechanical index level from 0.22 to 0.25, which is a low level in accordance with our previous report [22]. Gain was adjusted to an optimal level, and the dynamic range was set at 45–50 dB.

The contrast agent Sonazoid (perflubutane microbubbles with a median diameter of 2–3 μm) was used at a dose of 0.0075 ml/kg administered by manual bolus injection, followed by 3.0 ml of normal saline (administered by H.I.). Contrast enhancement was observed during two phases: the vascular phase (from contrast agent injection to 1 min, which is the early phase) and late phase (15 min after injection), under breath-holding as often as possible. For all patients, the operator performing the US examinations was M.T. (who had 7 years of experience in US examination). All US images recorded digitally were reviewed using frame-by-frame playback at a later date by H.M. (who had 19 years of experience in US examination), and contrast enhancement in the inner and outer nodules of the HCC lesions was assessed in comparison with that in adjacent liver parenchyma as hyper-, iso-, or hypo-enhanced in appearance.

### 2.3. Contrast-enhanced CT

Contrast-enhanced CT with dynamic imaging was performed in all patients using the Lightspeed Ultra16 (GE Yokogawa Medical Systems, Hino, Japan) with injection of 100 ml of contrast medium (Iopamiron 350; Nihon Schering, Osaka, Japan) at 3 ml/s into the antecubital vein by means of a mechanical injection system (Mark V ProVis, MEDRAD, Warrendale, PA, USA). Imaging was performed with a 30-s delay between contrast medium administration and start of imaging for the hepatic artery-dominant phase, 80-s delay for the portal vein-dominant phase, and 180-s delay for the equilibrium phase. The contrast-enhanced CT findings were evaluated by M.Y., who had 28 years of experience in heaptology, and was blinded to the patient information.

### 2.4. Pathological examination of HCC lesions

Pathological examination was performed on specimens obtained from 9 HCC lesions by percutaneous US-guided needle biopsy using a Sonopsy C1 needle (Hakko, Tokyo, Japan). Separate sampling from the inner and outer nodules was performed for 2 HCC lesions, although only a single sample was taken from the other 7 HCC lesions due to technical difficulties. All needle biopsies were performed by S.O. after US examination, and the time lag between contrast-enhanced US examination and needle biopsy ranged from 1 to 14 days (mean 4.5 ± 4.1 days). Pathological results were obtained from the surgically resected specimen in the case of one HCC lesion, with the time lag between contrast-enhanced US examination and surgical treatment being 2 months.

### 2.5. Statistical analysis

All data were expressed as means ± SD or percentages. Statistical significance was analyzed by using the Chi-square test, and $p$-values <0.05 were considered to be significant. Statistical analysis was performed using the SPSS software package (Version 13.0J; SPSS Inc., Chicago, IL, USA).

## 3. Results

### 3.1. Non-contrast US findings in HCC

Grey-scale US showed 5 lesions with a hyperechoic outer nodule and hypoechoic inner nodule, 2 lesions with a hypoechoic outer nodule and isoechoic inner nodule, one lesion with an isoechoic outer nodule and hypoechoic inner nodule, and one lesion with a hypoechoic outer nodule and hyperechoic inner nodule. In these 9 lesions, grey-scale US could clearly discriminate the outer nodule from the inner nodule, and the diameter of the inner nodules ranged from 6.6 to 16.0 mm (mean 10.9 ± 2.9 mm). The remaining lesion

**Table 1**
Pathological results and contrast enhancement of hepatocellular carcinoma.

| Case | Size (mm) | Pathology I/O | Inner nodule | | Outer nodule | |
|---|---|---|---|---|---|---|
| | | | V | L | V | L |
| 1 | 24 | M/W[a] | Hyper | Hypo | Hypo | Iso |
| 2 | 14.4 | W | Hyper | Hypo | Hypo | Iso |
| 3 | 23 | W | Hyper | Iso | Hypo | Iso |
| 4 | 39 | M/W[b] | Hyper | Hypo | Hypo | Iso |
| 5 | 25.1 | W | Hyper | Hypo | Hypo | Iso |
| 6 | 17.1 | W | Hyper | Hypo | Hyper | Hypo |
| 7 | 34.3 | M | Hyper | Hypo | Iso | Iso |
| 8 | 24.8 | W | Hyper | Hypo | Hyper | Hypo |
| 9 | 28.5 | W | Hyper | Iso | Iso | Iso |
| 10 | 31.1 | M/W[a] | Hyper | Hypo | Hyper | Hypo |

I/O: Inner nodule/outer nodule, V: vascular phase, L: late phase, W: well differentiated HCC, M: moderately differentiated HCC, Hyper: hyper-enhancement, Iso: iso-enhancement, Hypo: hypo-enhancement.
[a] Separate sampling for inner and outer nodules by needle biopsy.
[b] Assessment of pathological result on surgically resected specimen.

showed a hypoechoic appearance without any difference between the outer and inner nodules. Neither US nor contrast-enhanced CT detected ascites, vascular abnormality, portal vein thrombosis, or portal vein tumor thrombosis.

### 3.2. Contrast-enhanced US findings in HCC

Vascular-phase US images of the inner nodule were hyper-enhanced in appearance in all 10 lesions, and images of the outer nodule were hyper-enhanced in 3 lesions, iso-enhanced in 2, and hypo-enhanced in 5 (Table 1). As the contrast enhancement of the inner nodule was much stronger than that of the outer nodule in all lesions, dedifferentiation of the tumor was clearly demonstrated in this vascular phase. Late-phase images of the inner nodule showed a hypo-enhanced appearance in 8 lesions and iso-enhancement in 2. Meanwhile, late-phase images of the outer nodule were iso-enhanced in the 7 lesions that showed an iso- or hypo-enhanced appearance in the vascular phase, and hypo-enhanced in the 3 showing a hyper-enhanced appearance in the vascular phase (Tables 1 and 2 and Figs. 1 and 2). Neither the inner nodules nor the outer nodules had a hyper-enhanced appearance in the late phase. A late-phase hypo-enhanced appearance was significantly more frequent in the nodules showing early-phase hyper-enhancement (11/13) than in the nodules showing early-phase iso- or hypo-enhancement (0/7) in both the inner and outer nodules.

### 3.3. Pathological results and contrast enhancement in each nodule

Pathological examination of the 7 HCC lesions without separate nodule sampling revealed well-differentiated HCC in 6 lesions and moderately differentiated HCC in one. The remaining 3 lesions showed well-differentiated HCC in the outer nodule and moderately differentiated HCC in the inner nodule. Upon contrast-enhanced US, all inner nodules in the latter 3 lesions showed a hyper-enhanced appearance in the vascular phase and hypo-enhancement in the late phase. On the other hand, the outer nodule in 2 lesions showed a hypo-enhanced appearance in the vascular phase and iso-enhancement in the late phase, and that in one lesion showed a hyper-enhanced appearance in the vascular phase and hypo-enhancement in the late phase.

**Table 2**
Contrast enhancement in the outer and inner nodule.

| | Vascular phase (Hyper/Iso/Hypo) | Late phase (Hyper/Iso/Hypo) |
|---|---|---|
| Outer nodule | 3/2/5 | 0/7/3 |
| Inner nodule | 10/0/0 | 0/2/8 |

Hyper: Hyper-enhancement, Iso: iso-enhancement, Hypo: hypo-enhancement.

## 4. Discussion

The nodule-in-nodule appearance of HCC lesions, supported by radiological and pathological evidence, represents a characteristic feature of developing HCC [15–21]. Typical findings on contrast-enhanced CT/magnetic resonance imaging include a hypervascular spot within the iso- or hypo-vascular lesion. The outer nodule is generally considered to be at an earlier stage of carcinogenesis relative to the inner nodule in HCC, hence the nodule-in-nodule appearance.

A cardinal non-contrast US finding in HCC lesions with a nodule-in-nodule appearance is a hypoechoic nodule within a hyperechoic nodule, which was also the most common pattern in our study. However, as previously reported, focal hepatic lesions with nodule-in-nodule appearance show various patterns on the grey-scale sonogram, and one lesion in the current study appeared hypoechoic without showing any difference between the inner and outer nodules [23]. Therefore, hemodynamic-based imaging may be required to diagnose nodule-in-nodule-appearing tumors, and vascular-phase sonograms can be obtained easily with Sonazoid and have clearly demonstrated the difference in vascularity between the inner and outer nodules in HCC lesions, as in contrast-enhanced CT images. Similar to the results from previous studies using other kinds of microbubble contrast agents, the current study suggested that contrast-enhanced US with Sonazoid can offer at least the same rate of detecting characteristic HCC tumor vascularity as contrast-enhanced CT [24–26].

Late-phase appearance varied in the inner nodule, with 80% of nodules showing a hypo-enhanced appearance and 20% of nodules showing iso-enhancement. These results may be absolutely reasonable because late-phase wash-out following vascular-phase hyper-enhancement is considered to be typical findings in cases of HCC [11,12]. Meanwhile, outer nodules that were hypo- or iso-enhanced in the vascular phase showed an iso-enhanced appearance in the late phase, and those hyper-enhanced in the vascular phase showed hypo-enhancement in the late phase. As the inner nodule appears to be in the post-dedifferentiated state and thus in a more advanced stage of carcinogenesis relative to the outer nodule, it is logical to assume that, as HCC progresses, the inner nodule may eventually exhibit the same enhancement pattern seen later in the outer nodule. Thus, our results suggest that tumor neovascularity precedes the deficit in microbubble contrast accumulation during the dedifferentiation process of HCC. In fact, it is strongly speculated that developing HCC progresses from lesions with hypo- or iso-enhancement in the vascular phase and iso-enhancement in the late phase, to lesions with hyper-enhancement in the vascular phase and iso-enhancement in the late phase, and subsequently to lesions with hyper-enhancement in the vascular phase and hypo-enhancement in the late phase. Therefore, a late-phase observation alone may not always be sufficient in screening for HCC because it could fail to detect developing HCC with an iso-enhanced appearance in the late phase.

Phagocytosis of microbubbles by Kupffer cells is one of the theoretical mechanisms for the late-phase enhancement findings in contrast-enhanced US with Sonazoid [14]. Considering the relationship between Kupffer cell distribution and cellular differentiation in HCC, the microbubble-related enhancement patterns in the late phase in our study might be explained by this theory [5,6]. The Levovist contrast agent also accumulates in the liver, and it is

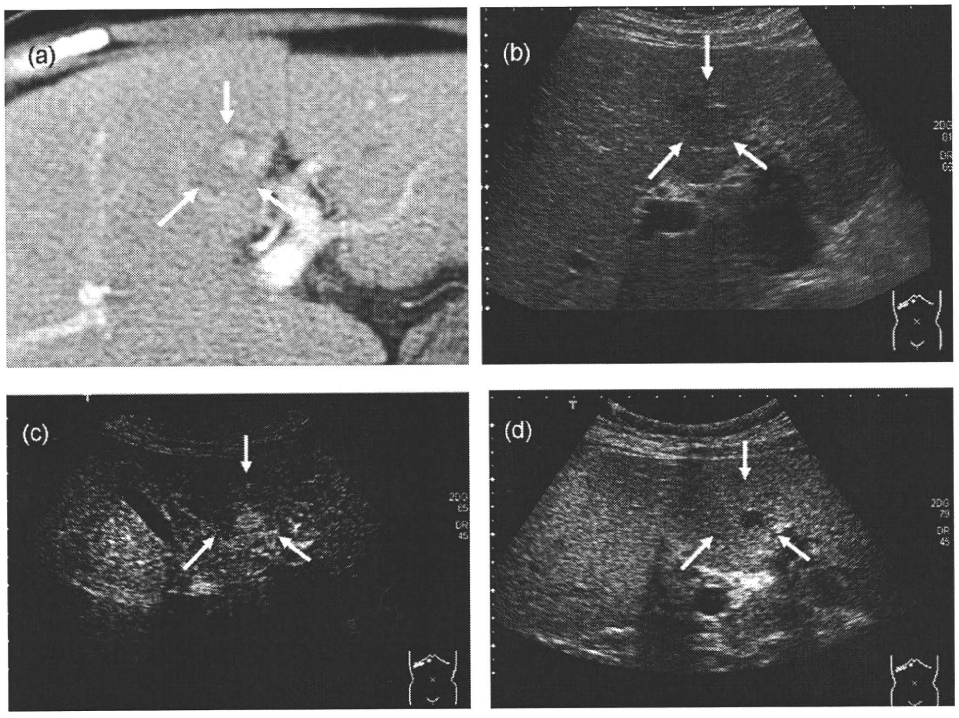


**Fig. 1.** A 69-year-old female, hepatitis C virus-related cirrhosis, HCC with nodule-in-nodule appearance (S4, 24 mm; case 1). (a) Contrast-enhanced CT, artery-dominant phase. HCC with hypovascular outer nodule and hypervascular inner nodule (arrows). (b) Grey-scale US. HCC with hypoechoic appearance (arrows). (c) Contrast-enhanced US, vascular phase. HCC with hypo-enhanced outer nodule and hyper-enhanced inner nodule (arrows). (d) Contrast-enhanced US, late phase. HCC with iso-enhanced outer nodule and hypo-enhanced inner nodule (arrows).

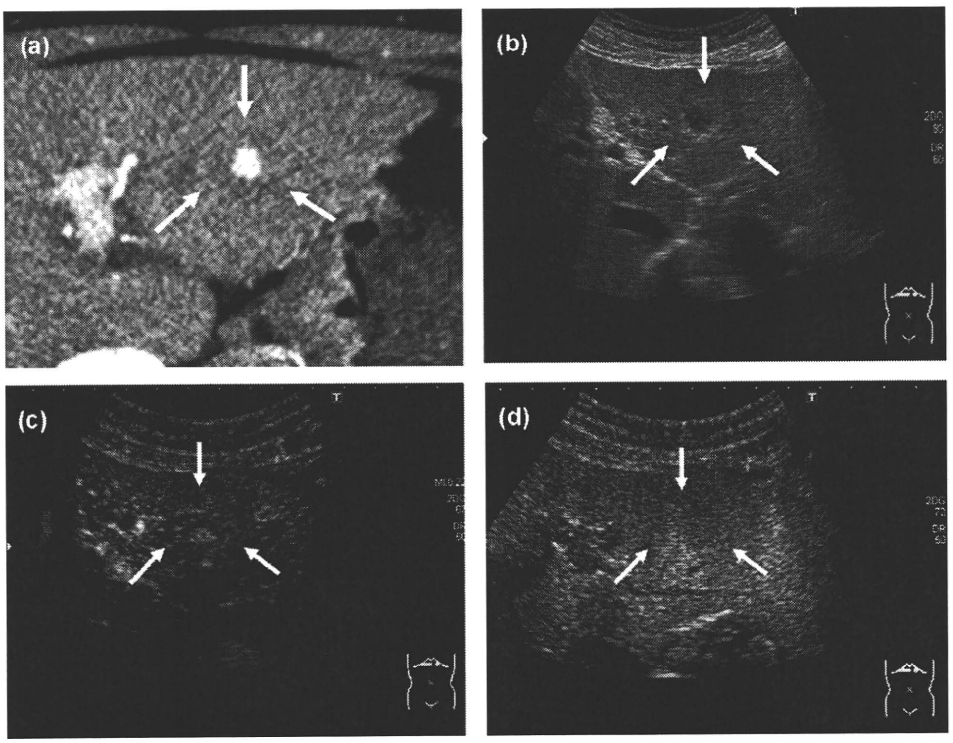


**Fig. 2.** A 74-year-old female, hepatitis C virus-related cirrhosis, HCC with nodule-in-nodule appearance (S3, 28.5 mm; case 9). (a) Contrast-enhanced CT, artery-dominant phase. HCC with isovascular outer nodule and hypervascular inner nodule (arrows). (b) Grey-scale US. HCC with hyperechoic outer nodule and hypoechoic inner nodule (arrows). (c) Contrast-enhanced US, vascular phase. HCC with iso-enhanced outer nodule and hyper-enhanced inner nodule (arrows). (d) Contrast-enhanced US, late phase. HCC with iso-enhanced outer and inner nodules (arrows).

reported that late-phase enhancement with this agent in well-differentiated HCC and benign regenerative nodules was similar to that in adjacent non-tumor liver parenchyma, whereas moderately differentiated HCC tended to have a washed-out appearance in this phase [11,12,27]. Meanwhile, in studies using the contrast agents SonoVue® (Bracco, Milan, Italy) and Definity® (Lantheus, North Billerica, MA, USA), which do not accumulate in the liver, hypo-enhancement or a washed-out appearance after the vascular-phase peak enhancement and an earlier wash-out were frequent and consistent with the degree of tumor differentiation in HCC [28,29]. These results with different contrast agents suggest that hypo-enhancement or wash-out findings may be common in spite of the type of US contrast agent used, and mechanisms other than Kupffer cell distribution might account for the late-phase enhancement pattern in HCC. However, as these possible explanations are still at a speculative level, further investigations are required to account for these findings.

Our study had several limitations. The first is that the histological results of all but one HCC were obtained from specimens obtained by percutaneous US-guided needle biopsy, and separate sampling from inner and outer nodules was performed in only 2 of the 9 HCC lesions biopsied. According to previous studies, the histological structure of the outer nodule in nodule-in-nodule-appearing lesions varies and can be diagnosed as: adenomatous hyperplasia, siderotic regenerative nodule, macroregenerative nodule, or well-differentiated HCC [15–19]. Assessment of the pathology of the surgically resected specimen might allow confirmation of agreement between the histological findings and the results of US with contrast enhancement. The second limitation is that our study consisted of a small number of subjects and lacked follow-up of the natural progression of HCC with nodule-in-nodule appearance. Further studies with large numbers of patients and with US follow-up of contrast-enhanced changes in each nodule during the period between diagnosis and treatment may be necessary to allow us to draw more definitive conclusions.

## 5. Conclusions

Dedifferentiation of HCC may be accompanied by changes in neovascularity prior to the reduction in microbubble contrast accumulation, with the latter possibly related to Kupffer cell distribution. Although late-phase ultrasonography with static microbubbles may have the advantage of easy and stable observation, vascular-phase contrast enhancement using Sonazoid dynamic microbubbles could allow early recognition of the dedifferentiation of HCC.

## References


[1] Bosch FX, Ribes J, Borras J. Epidermiology of primary liver cancer. Semin Liver Dis 1999;19(3):271–85.
[2] Okuda K. Hepatocellular carcinoma. J Hepatol 2000;32(1 Suppl.):225–37.
[3] Tong MJ, Blatt LM, Kao VW. Surveillance for hepatocellular carcinoma in patients with chronic viral hepatitis in the United States of America. J Gastroenterol Hepatol 2001;16(7):553–9.
[4] Larcos G, Sorokopud H, Berry G, Farrell GC. Sonographic screening for hepatocellular carcinoma in patients with chronic hepatitis or cirrhosis: an evaluation. AJR Am J Roentgenol 1998;171(2):433–5.
[5] Tanaka M, Nakashima O, Wada Y, Kage M, Kojiro M. Pathomorphological study of Kuppfer cells in hepatocellular carcinoma and hyperplastic nodular lesions in the liver. Hepatology 1996;24(4):807–12.
[6] Imai Y, Murakami T, Yoshida S, et al. Super paramagnetic iron oxide enhanced magnetic resonance images of hepatocellular carcinoma: correlation with histological grading. Hepatology 2000;32(2):205–12.
[7] Hayashi M, Matsui O, Ueda K, et al. Correlation between the blood supply and grade of malignancy of hepatocellular nodules associated with liver cirrhosis: evaluation by CT during intraarterial injection of contrast medium. Am J Roentgenol 1999;172(4):969–76.
[8] Kremkau FW. Diagnostic ultrasound: principles and instruments. 4th ed. Philadelphia: WB Saunders; 1993.
[9] Mitchell DG. Color Doppler imaging: principles, limitations, and artifacts. Radiology 1990;177(1):1–10.
[10] Goldberg BB. Ultrasound contrast agents. Martin Dunitz Ltd.; 1997.
[11] Rettenbacher T. Focal liver lesions: role of contrast-enhanced ultrasound. Eur J Radiol 2007;64(2):173–82.
[12] Quaia E. Microbubble ultrasound contrast agents: an update. Eur Radiol 2007;17(8):1995–2008.
[13] Marelli C. Preliminary experience with NC100100, a new ultrasound contrast agent for intravenous injection. Eur Radiol 1999;9(Suppl. 3):S343–6.
[14] Watanabe R, Matsumura M, Munemasa T, Fujimaki M, Suematsu M. Mechanism of hepatic parenchyma-specific contrast of microbubble-based contrast agent for ultrasonography: microscopic studies in rat liver. Invest Radiol 2007;42(9):643–51.
[15] Matsui O, Kadoya M, Kameyama T, et al. Adenomatous hyperplastic nodules in the cirrhotic liver: differentiation from hepatocellular carcinoma with MR imaging. Radiology 1989;173(1):123–6.
[16] Mitchell DG, Rubin R, Siegelman ES, Burk Jr DL, Rifkin MD. Hepatocellular carcinoma within siderotic regenerative nodules: appearance as a nodule within a nodule on MR images. Radiology 1991;178(1):101–3.
[17] Muramatsu Y, Nawano S, Takayasu K, et al. Early hepatocellular carcinoma: MR imaging. Radiology 1991;181(1):209–13.
[18] Winter 3rd TC, Takayasu K, Muramatsu Y, et al. Early advanced hepatocellular carcinoma: evaluation of CT and MR appearance with pathologic correlation. Radiology 1994;192(2):379–87.
[19] Sadek AG, Mitchell DG, Siegelman ES, Outwater EK, Matteucci T, Hann HW. Early Hepatocellular carcinoma that develops within macroregenerative nodules: growth rate depicted at serial MR imaging. Radiology 1995;195(3):753–6.
[20] Kojiro M. 'Nodule-in-nodule' appearance in hepatocellular carcinoma: its significance as a morphologic marker of dedifferentiation. Intervirology 2004;47(3–5):179–83.
[21] Zheng RQ, Zhou P, Kudo M. Hepatocellular carcinoma with nodule-in-nodule appearance: demonstration by contrast-enhanced coded phase inversion harmonic imaging. Intervirology 2004;47(3–5):184–90.
[22] Maruyama H, Takahashi M, Ishibashi H, et al. Ultrasound-guided treatments under low acoustic power contrast harmonic imaging for hepatocellular carcinomas undetected by B-mode ultrasonography. Liver Int 2009;29(5):708–14.
[23] Ishida Y, Nagamatsu H, Koga H, Yoshida H, Kojiro M, Sata M. Hepatocellular carcinoma with a "nodule-in-nodule" appearance reflecting an unusual dilated pseudoglandular structure. Int Med 2008;47(13):1215–8.
[24] Numata K, Tanaka K, Kiba T, et al. Contrast-enhanced, wide-band harmonic gray scale imaging of hepatocellular carcinoma. Correlation with helical computed tomographic findings. J Ultrasound Med 2001;20(2):89–98.
[25] Giorgio A, Ferraioli G, Tarantino L, et al. Contrast-enhanced sonographic appearance of hepatocellular carcinoma in patients with cirrhosis: comparison with contrast-enhanced helical CT appearance. AJR Am J Roentgenol 2004;183(5):1319–26.
[26] Bolondi L, Gaiani S, Celli N, et al. Characterization of small nodules in cirrhosis by assessment of vascularity: the problem of hypovascular hepatocellular carcinoma. Hepatology 2005;42(1):27–34.
[27] Yoshizumi H, Maruyama H, Okugawa H, et al. How to characterize non-hypervascular hepatic nodules on contrast-enhanced computed tomography in chronic liver disease: feasibility of contrast-enhanced ultrasound with a microbubble contrast agent. J Gastroenterol Hepatol 2008;23(10):1528–34.
[28] Nicolau C, Catalá V, Vilana R, et al. Evaluation of hepatocellular carcinoma using SonoVue, a second generation ultrasound contrast agent: correlation with cellular differentiation. Eur Radiol 2004;14(6):1092–9.
[29] Jang HJ, Kim TK, Burns PN, Wilson SR. Enhancement pattern of hepatocellular carcinoma at contrast-enhanced US: comparison with histologic differentiation. Radiology 2007;244(3):898–906.

European Journal of Radiology 75 (2010) e41–e45

Contents lists available at ScienceDirect

European Journal of Radiology

journal homepage: www.elsevier.com/locate/ejrad

# Blood flow parameters in the short gastric vein and splenic vein on Doppler ultrasound reflect gastric variceal bleeding

Hitoshi Maruyama*, Takeshi Ishihara, Hiroshi Ishii, Toshio Tsuyuguchi, Masaharu Yoshikawa, Shoichi Matsutani, Osamu Yokosuka

*Department of Medicine and Clinical Oncology, Chiba University Graduate School of Medicine, 1-8-1, Inohana, Chuou-ku, Chiba 260-8670, Japan*

ARTICLE INFO

*Article history:*
Received 11 May 2009
Accepted 22 June 2009

*Keywords:*
Gastric varices
Short gastric vein
Splenic vein
Portal hypertension
Doppler ultrasound

ABSTRACT

*Purpose:* Hemodynamic features associated with the bleeding from gastric fundal varices (FV) have not been fully examined. The purpose of this study was to elucidate hemodynamics in the short gastric vein (SGV) which is a major inflow route for FV and flow direction of the splenic vein (SV) in relation to bleeding FV.

*Materials and Methods:* The subject of this retrospective study was 54 cirrhotic patients who had medium- or large-sized FV (20 bleeders, 34 non-bleeders) on endoscopy with SGV on both angiogram and sonogram. Diameter, flow velocity, flow volume of SGV and flow direction in the SV were evaluated by Doppler ultrasound.

*Results:* Diameter, flow velocity and flow volume of SGV were significantly greater in bleeders ($9.6 \pm 3.1$ mm, $11.4 \pm 5.2$ cm/s, $499 \pm 250.1$ ml/min) than non-bleeders ($6.5 \pm 2.2$ mm, $p = 0.0141$; $7.9 \pm 3.3$ cm/s, $p = 0.022$; $205 \pm 129.1$ ml/min, $p = 0.0031$). SV showed forward flow in 37 (68.5%), to and fro in 3 (5.6%) and reversed flow in 14 patients (25.9%). The frequency of FV bleeding was significantly higher in case with reversed or "to and fro" SV flow (11/17) than forward SV flow (9/37, $p = 0.0043$). The cumulative bleeding rate at 3 and 5 years was significantly higher in patients without forward SV flow (38.8% at 3 years, 59.2% at 5 years) than in patients with forward SV flow (18.7% at 3 years, 32.2% at 5 years, $p = 0.0199$).

*Conclusion:* Advanced SGV blood flow and reversed SV flow direction may be a hemodynamic features closely related to the FV bleeding.



## 1. Introduction

Gastric fundal varices (FV) are well known as a considerable hemodynamic feature in patients with portal hypertension [1–3]. Although the incidence is less than that of esophageal varices (EV), they provide a large hemorrhage volume, resulting in a serious condition in case of bleeding [4–6]. Management of bleeding FV is actually important issue for the clinicians.

Hepatic functional reserve, size of varices, and red spots on varices by endoscopic examination were reported as significant factors for FV bleeding [5,7]. However, as these parameters are not quantitatively well defined, they are not always satisfactory in clinical practice. Although portal venous pressure (PVP) also accounts for the FV bleeding, measurement of PVP still requires an invasive procedure and patients without high PVP sometimes present developed FV or FV bleeding [8,9]. Pathophysiological difference in the FV between bleeders and non-bleeders has not been fully resolved.

Portal hypertension frequently results in the development of collateral vessels and a change in blood flow direction. Left gastric vein (LGV) supplies blood flow for EV, and its hemodynamics reflect the grade and bleeding of EV [10–12]. Similarly, gastric veins such as LGV, short gastric vein (SGV) and posterior gastric vein (PGV) are known as inflow routes for FV, and hemodynamics of these vessels might be closely related to the pathophysiology of FV [13,14]. Additionally, it is reported that reversed flow of splenic vein (SV) was frequent in patients with advanced FV accompanied by chronic portal systemic encephalopathy [13]. Blood flow in the SV might also reflect the potential development of FV.

Pulsed and color Doppler ultrasound (US) has the advantage of allowing real-time observation of the portal hemodynamics in patients with portal hypertension, repeatedly and non-invasively, compared with other imaging modalities [15–18]. With the use of

* Corresponding author. Tel.: +81 43 2262083; fax: +81 43 2262088.
*E-mail addresses:* maru-cib@umin.ac.jp (H. Maruyama), ishihara@faculty.chiba-u.jp (T. Ishihara), hiroshi.ishii@jfcr.or.jp (H. Ishii), tsuyuguchi@faculty.chiba-u.jp (T. Tsuyuguchi), yoshikawa@faculty.chiba-u.jp (M. Yoshikawa), shoichi.matsutani@cchs.ac.jp (S. Matsutani), yokosukao@faculty.chiba-u.jp (O. Yokosuka).

0720-048X/$ – see front matter © 2009 Elsevier Ireland Ltd. All rights reserved.
doi:10.1016/j.ejrad.2009.06.024

these US techniques, we focused on the hemodynamics of the SGV and flow direction in the SV in FV patients. The purpose of our study was to elucidate the hemodynamic features of the SGV and SV on Doppler sonograms in relation to the bleeding FV.

## 2. Patients and methods

### 2.1. Patients

There were 149 consecutive patients who had medium- or large-sized FV on endoscopic examination in our department between April 1994 and December 2003. Among them, this retrospective study enrolled subjects according to the following criteria; (i) subjects received angiographic examination, that is arterial portography for the treatment of HCC or percutaneous transhepatic portography (PTP) for the portal hemodynamic evaluation, 72/149, (ii) subjects who had SGV as inflow route for FV on the angiogram, 62/72, (iii) subjects underwent Doppler US examination for the portal hemodynamic evaluation prior to treatments for FV, 59/62, (iv) subjects who had SGV on Doppler US, 54/59. Therefore, the subjects were 54 patients who consisted of 34 males and 20 females, aged 37–79 years (63.8 ± 8.2). All subjects were diagnosed as cirrhosis on the basis of imaging findings with clinical symptoms and biochemistry findings. The cause of cirrhosis was viral in 40 patients (hepatitis C virus 33, hepatitis B virus 7), alcohol abuse in 7, cryptogenic in 5 and primary biliary cirrhosis in 2. The severity of liver dysfunction as classified by the Child-Pugh scoring system was A in 18, B in 19, and C in 17. Forty-two patients had hepatocellular carcinomas (HCCs), which were controlled by non-surgical treatment. None had thrombosis or tumor thrombosis in the portal vein on both the sonogram and angiogram. The beginning of follow-up period was the time of initial Doppler US examination, and the end of that was bleeding from FV, death, changing hospital or denial to hospital visit, or the time of the latest Doppler US observation. The duration of clinical observation of FV was 18–4380 (1159 ± 1088) days in this study. The informed written consent was obtained from all patients, and the research was carried out in accordance with the Helsinki Declaration. The ethics committee in our hospital deemed this retrospective study as an appropriate design for the publication.

### 2.2. Endoscopy

Endoscopic findings of FV and EV were classified according to the General Rules for Recording Endoscopic Findings set by the Japan Research Society for Portal Hypertension [19]: F1 (straight), F2 (winding), and F3 (nodule-beaded), corresponding to the grades of small, medium and large, respectively. The grades of FV were F2 in 32, and F3 in 22; 12 of the FV patients were accompanied by EV (F1 in 5 and F2 in 7). Twenty FV patients were bleeders: 12 confirmed by emergency endoscopy and 6 of them received endoscopic sclerotherapy after the Doppler US examination, and 8 by clinical symptoms of hematemesis or melena. The latter patients underwent endoscopic examination within 10 days after appearance of symptoms, and other causes for gastrointestinal bleeding were not found except for FV. The other thirty-four FV patients were non-bleeders with no history of hematemesis or melena. Endoscopic examination was performed by HI, TI and TT.

### 2.3. US examination

The US system used in our study was SSA-260A, 270A and 390A (Toshiba, Tokyo, Japan) with a 3.75-MHz convex probe. The imaging modes were fundamental grey-scale imaging, pulsed and color Doppler US. The fundamental grey-scale imaging was used for the measurement of maximum diameter of the vessels, and Doppler US

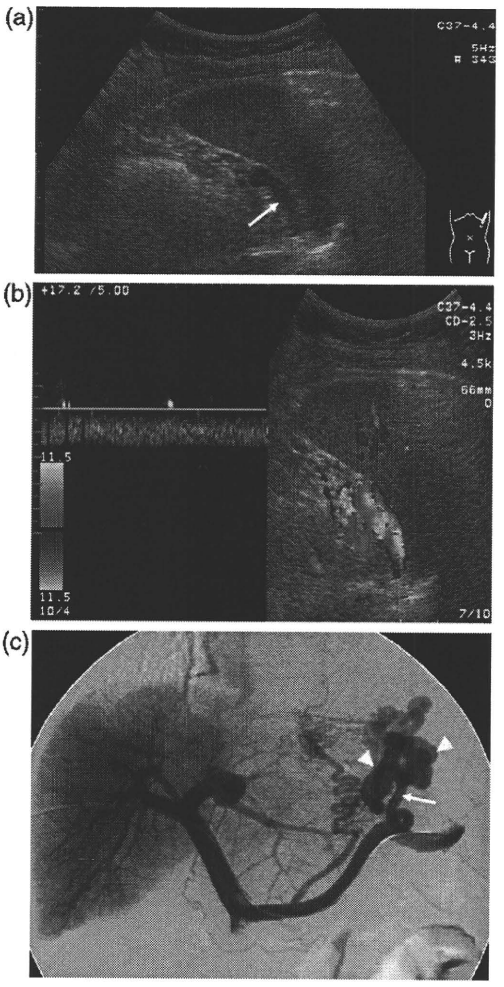


**Fig. 1.** 59-year-old female, cirrhotic patient with FV. (a) B-mode US by left intercostal scan. The short gastric vein (SGV, arrow) was demonstrated beside the spleen by left intercostal scan. (b) Pulsed and color Doppler US by left intercostal scan. Flow direction of SGV was hepatofugal. (c) Portogram. SGV (arrow) was observed running toward the FV (arrow heads). FV, gastric fundal varices.

was used for the demonstration of the flow direction, and measurement of mean flow velocity (cm/s) and mean flow volume (ml/min) calculated by multiplying mean flow velocity by cross-section of the vessel by 60 (s) automatically, with sampling width corresponding to the diameter of the vessel. Care was taken to ensure that the angle between the US beam and the vessel was less than 60° in this study. Color Doppler US was done with an optimal level of gain and at 60–65 dB of dynamic range, and these settings were used in all examinations. US examination was performed in a supine position in an intermediate or inspiratory phase of respiration with a fasting state of over 6 h except for the emergency setting in bleeders. The observation for SGV was performed under left intercostal scan or subcostal scan, and SGV was defined as collateral vessels originating from the splenic hilum, running along the splenic surface in a hepatofugal flow direction (Fig. 1a, b) [18,20]. The SV was observed under the transverse scan in the middle part of the upper abdomen.

The US examination was performed by two operators who had more than 5-year career for Doppler US examination at the observation of the initial case, SM for 36 patients and HM for 32 patients. Therefore, 14 patients received US examination by two operators independently, and inter-observer variability of measurement data

**Table 1**
Flow direction in the SV in relation to the bleeding from FV.

| | Bleeder | Non-bleeder |
|---|---|---|
| Forward flow | 9 | 28 |
| Reversed flow[a] | 11 | 6 |

$p = 0.0043$ (Chi square test); SV, splenic vein; FV, gastric fundal varices.
[a] SV with "to and fro" direction in three cases, bleeder in 2 and non-bleeder in 1.

was evaluated in them, given as a coefficient of variation, calculated by dividing the standard deviation (SD) by mean and multiplying by 100. The number of US examinations of each patient was 1.9 ± 1.9 (1–13 times) during the clinical course.

### 2.4. Angiography

A portogram was obtained by arterial portography or PTP. The former was performed by MY by means of superior mesenteric arteriography and celiac arteriography using a 5-Fr catheter with rapid injection of iodinated contrast material (30 ml at 5 ml/s), and the latter by HM under US-guided procedure with rapid injection of iodinated contrast material (35 ml at 7 ml/s) into the splenic hilum. Arterial portography was performed in 42 patients who underwent the treatment of HCC, and PTP was done for the evaluation of portal hemodynamics in 12 patients who had neither ascites nor HCC. All of them were done before the Doppler US examination, and the presence or absence of SGV on the portograms were blindly reviewed by SM (Fig. 1c).

### 2.5. Statistical analysis

All results were expressed as mean ± SD or percentage. Statistical significance of differences in diameter, flow velocity and flow volume of SGV between bleeder and non-bleeder was assessed using Mann–Whitney U-test. Chi square test was used for the comparison of the SV flow direction between bleeders and non-bleeders. The cumulative bleeding rate was calculated by the Kaplan–Meier method and the difference in relation to the SV flow direction was compared by Log-rank test. Statistical analysis was performed using the Dr. SPSS package (version 11.0J for Windows; SPSS Inc., Chicago, Illinois, USA). $p$ values of less than 0.05 were considered to indicate statistical significance.

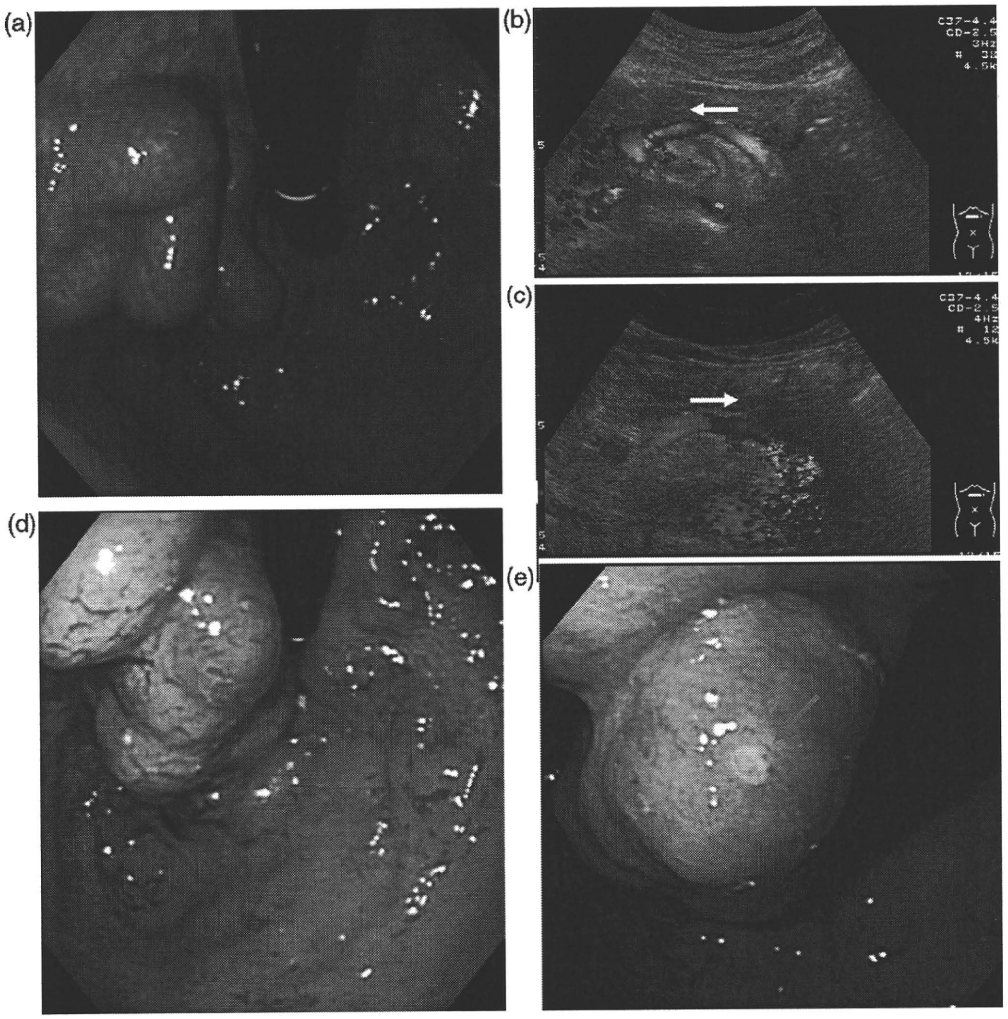


**Fig. 2.** 64-year-old male, cirrhotic patient with FV. (a) Endoscopic findings on July 30th, 1997. Endoscopy showed medium-sized FV. (b) Doppler US findings by transverse scan on July 30th, 1997. Flow direction of SV was forward (arrow, flow direction). (c) Doppler US findings by transverse scan on February 19th, 2001. Flow direction of SV was reversed (arrow, flow direction). (d) Endoscopic findings on March 15th, 2001. (e) Endoscopic findings on March 15th, 2001. Bleeding from gastric fundal varices (arrow: bleeding point) was noted, after 25 days of the last Doppler US examination. FV, gastric fundal varices; SV, splenic vein.